Teh, C. I. & Houlsby, G. T. (1991). *Géotechnique* **41**, No. 1, 17–34

An analytical study of the cone penetration test in clay

C. I. TEH* and G. T. HOULSBY†

This Paper describes an analysis of the quasi-static penetration of a cone penetrometer into clay. The clay is idealized as a homogeneous elastic–perfectly plastic material obeying the von Mises yield criterion. The analysis is based on the strain path method, with an additional equilibrium correction provided by large strain finite element analysis. The dissipation of excess pore water pressure is analysed using uncoupled Terzaghi–Rendulic consolidation theory. The primary importance of the rigidity index and of the horizontal stress in influencing the cone factor N_{kt}, is emphasized and an equation relating N_{kt} to soil parameters and cone roughness is proposed. Based on finite difference analysis of the pore pressure dissipation around the cone, a new interpretation method for consolidation data from a piezocone is suggested.

KEYWORDS: clays; consolidation; field tests; finite elements; plasticity; stress analysis.

Cet article décrit une analyse de la pénétration quasi-statique d'un pénétromètre dans l'argile. L'argile est considérée de façon idéalle comme une matière homogène élastique parfaitement plastique et qui satisfait le critère d'écoulement de von Mises. L'analyse est basée sur la méthode des chemins de déformation, avec une correction supplémentaire de l'équilibre fournie par l'analyse en éléments finis des déformations importantes. À l'aide de la théorie de consolidation non-couplée de Terzaghi–Rendulic on analyse la dissipation de la pression excédentaire de l'eau interstitielle. L'article souligne l'influence essentielle exercée sur le facteur de cône N_{kt} par l'indice de rigidité et la contrainte horizontale. Il est proposée une équation qui lie N_{kt} aux paramètres de sol et à la rugosité du cône. On propose une nouvelle méthode d'interprétation des données de consolidation à partir du piezocône basée sur l'analyse différentielle finie de la dissipation de la pression de l'eau interstitielle.

INTRODUCTION

This Paper presents in outline a method of analysis used to study the penetration of a piezocone into clay. The full analysis consists of two stages. In the first the undrained penetration of the cone penetrometer into clay is analysed, with the clay idealized as an incompressible elastic–perfectly plastic (or von Mises) material. The soil displacement and stress changes around the cone are computed and values of the cone factor N_{kt} are derived. A parametric study of the various factors which influence the cone factor is carried out. In the second stage the consolidation around a static cone is analysed using uncoupled Terzaghi–Rendulic consolidation theory. This involves a straighforward solution of the diffusion equation in axial symmetry. An alternating direction, implicit finite difference scheme is adopted. A more rigorous analysis of the consolidation phase is planned as a future research project.

Discussion on this Paper closes 5 July 1991; for further details see p. ii.

* CAD/CAM Specialist, Faculty of Engineering, National University of Singapore, 10 Kent Ridge Crescent, Singapore 0511.

† Department of Engineering Science, Oxford University, Parks Road, Oxford OX1 3PJ.

METHOD OF ANALYSIS FOR CONE PENETRATION

Various analytical methods have been proposed for the penetration problem in the past. These can broadly be divided into two main classes, namely bearing capacity theories and cavity expansion theories. Very often the results of plane strain bearing capacity calculations are modified empirically for application to the axially symmetric problem. Some numerical solutions to axisymmetric problems using plasticity theory have also been presented (e.g. Cox *et al.*, 1961; Houlsby & Wroth, 1983). Adaptation of bearing capacity theory to deep penetration problems is much more difficult and often involves adoption of boundary conditions which are not appropriate for conventional cone penetrometers (e.g. Koumoto & Kaku, 1982). However, when the correct boundary conditions are imposed, bearing capacity theory leads to cone factors which increase indefinitely with increased penetration (Houlsby & Wroth, 1982). In practice, empirical depth factors are usually applied to shallow bearing capacity solutions for the interpretation of cone data.

The problem of the transition between shallow and deep penetration is readily explained by the fact that shallow penetration involves a mecha-

nism in which the displaced material moves almost entirely outwards and upwards to the free surface, while in deep penetration the displaced material is accommodated by elastic deformation of the soil. Thus, cavity expansion theories have been suggested as being appropriate for the deep penetration problem (Vesic, 1972). It is widely held that the limit solution for the cylindrical cavity pressure Ψ_c is applicable to the estimation of the radial stress on the penetrometer shaft, and the limit pressure for spherical cavity expansion Ψ_s is relevant to the end bearing of the cone.

For a von Mises material with the yield condition defined as

$$(\sigma_{rr} - \sigma_{\theta\theta})^2 + (\sigma_{\theta\theta} - \sigma_{zz})^2 + (\sigma_{zz} - \sigma_{rr})^2 + 6\tau_{rz}^2 = 8s_u^2 \quad (1)$$

the limit pressure in expanding a cylindrical cavity is

$$\Psi_c = \sigma_{ro} + \frac{2s_u}{\sqrt{3}}\left[1 + \ln\left(\frac{\sqrt{3}}{2} I_r\right)\right] \quad (2)$$

where the rigidity index of soil I_r is defined as G/s_u. Note that s_u is the undrained strength in triaxial compression and G is the shear modulus. The von Mises criterion as expressed in equation (1) implies a shear strength in plane strain of $(2/\sqrt{3})s_u$.

The spherical cavity expansion pressure is often considered as an estimate of the pressure at the cone tip. For the von Mises criterion this limit pressure is given by

$$\Psi_s = \sigma_{ro} + \frac{4s_u}{3}[1 + \ln(I_r)] \quad (3)$$

Baligh (1986) has pointed out that one of the inconsistencies in the application of the cavity expansion theory to cone penetration problems is that it does not model correctly the strain paths followed by soil elements. He suggested the use of the strain path method for problems of deep steady penetration. This method attempts to account for the complex deformation history of the soil during cone penetration. In this study the cone penetration problem in clay is analysed using the strain path method. Instead of attempting to reproduce an approximate penetrometer geometry by a combination of sources and sinks in a uniform flow field (Baligh, 1985) the actual geometry of the penetrometer is included explicitly in the analysis. The governing equation is formulated and solved using the finite difference method. Fig. 1 shows a typical finite difference mesh used in the present study.

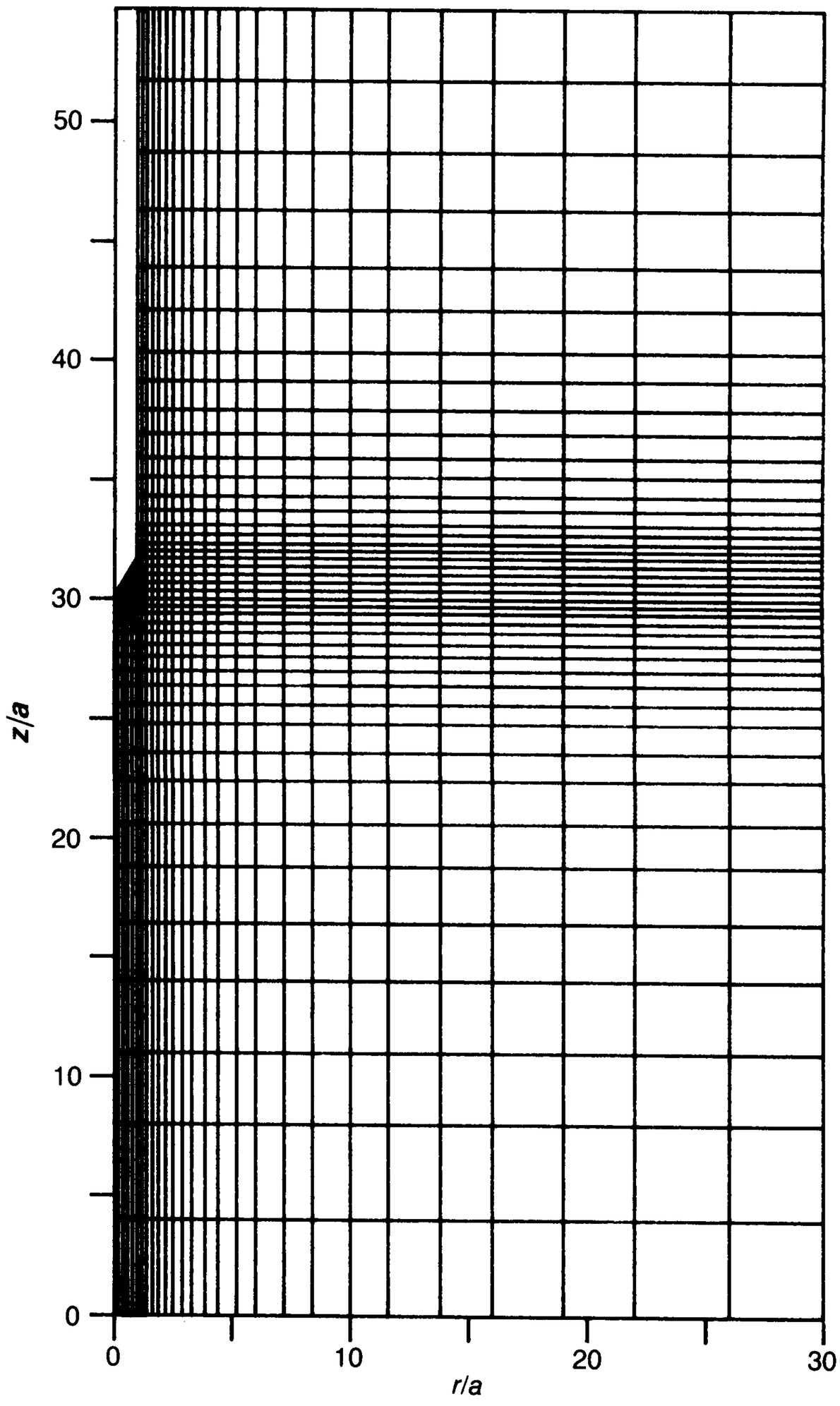

Fig. 1. Finite difference mesh for strain path analysis

THE STRAIN PATH METHOD

The steady penetration of a cone in a homogeneous material is a quasi-static problem. By changing the frame of reference the penetration process can be viewed as a steady flow of soil past a stationary penetrometer. An initial estimate of the flow field must be made. In the present study this estimate is obtained by assuming the soil to flow like a viscous fluid. The flow pattern thus obtained is of course slightly in error since an incorrect constitutive law has been used. But because the problem is heavily constrained kinematically (by the incompressibility condition and the boundary conditions on the cone) this estimate represents a reasonable first approximation. From the computed flow pattern the complete history of strain for each soil element may be determined.

Using appropriate initial stresses (which may be anisotropic) for the soil, the deviatoric stresses may be determined by integration of the appropriate constitutive laws along the streamlines. In this study a simple linear elastic–perfectly plastic model with a von Mises yield surface was used.

This particular constitutive relation involves only two material parameters, the shear modulus G and the shear strength in triaxial compression s_u (see equation (1)). Adopting this behavioural model for clay, which is expressed in terms of total (not effective) stresses, the appropriate incremental equations for the steady flow problem (Houlsby *et al.*, 1985) are given by

$$\dot{\varepsilon}_{rr} = \frac{\partial u}{\partial r} = \frac{1}{2G}\dot{\sigma}_{rr}' + 6\lambda\sigma_{rr}' \tag{4}$$

$$\dot{\varepsilon}_{zz} = \frac{\partial v}{\partial z} = \frac{1}{2G}\dot{\sigma}_{zz}' + 6\lambda\sigma_{zz}' \tag{5}$$

$$\dot{\varepsilon}_{rr} = \frac{\partial u}{\partial r} = \frac{1}{2G}\dot{\sigma}_{\theta\theta}' + 6\lambda\sigma_{\theta\theta}' \tag{6}$$

$$\dot{\gamma}_{rz} = \frac{\partial v}{\partial r} + \frac{\partial u}{\partial z} = \frac{1}{G}\dot{\tau}_{rz} + 12\lambda\tau_{rz} \tag{7}$$

where u and v are the velocities in the r (radial) and z (axial) directions respectively, and λ is the plastic multiplier. A superposed dot denotes the time differential and a prime indicates the deviatoric components, e.g.

$$\sigma_{rr}' = \sigma_{rr} - p \tag{8}$$

where

$$p = \tfrac{1}{3}(\sigma_{rr} + \sigma_{\theta\theta} + \sigma_{zz}) \tag{9}$$

Compressive stresses and strains are taken as positive in this study.

The velocities in equations (4) to (7) must be such that the incompressibility condition is satisfied. This is most conveniently achieved by defining the velocities in terms of a potential function Ψ

$$u = \frac{1}{r}\frac{\partial \Psi}{\partial z}, \qquad v = -\frac{1}{r}\frac{\partial \Psi}{\partial r} \tag{10}$$

The stress rates in steady flow are given by the convective equation

$$\dot{\sigma}_{rr}' = u\frac{\partial \sigma_{rr}'}{\partial r} + v\frac{\partial \sigma_{rr}'}{\partial z} \tag{11}$$

and three analogous equations for $\dot{\sigma}_{zz}'$, $\dot{\sigma}_{\theta\theta}'$ and $\dot{\tau}_{rz}$. These equations are supplemented by either $\lambda = 0$ for elastic behaviour if the stresses are within the yield surface or equation (1) in the case of plastic deformation. In addition, the equilibrium equations

$$\frac{\partial \sigma_{rr}}{\partial r} + \frac{\partial \tau_{rz}}{\partial z} + \frac{\sigma_{rr} - \sigma_{\theta\theta}}{r} = 0 \tag{12}$$

$$\frac{\partial \sigma_{zz}}{\partial z} + \frac{\partial \tau_{rz}}{\partial r} + \frac{\tau_{rz}}{r} = 0 \tag{13}$$

must be satisfied. It should be noted that while a simple constitutive rule has been used in this analysis, alternative models for the deviatoric stress–strain behaviour could easily be included in the method.

For an incompressible material the mean stress p is not determined by the constitutive equation but appears as a reaction which is determined solely by the equilibrium equations. Therefore, having calculated the deviatoric stresses the mean normal stress may be determined by using one of the equations of equilibrium (radial or axial) and integration from an outer boundary (which must be set at some point sufficiently distant from the cone). However, in general the stresses so computed do not exactly satisfy the other equilibrium equation. The discrepancy reflects the error in the initial flow field. In principle the remaining relationship could be used to correct the flow field. Some iterative schemes to attempt this correction are presented in Appendix 1. While some of these schemes are effective in reducing the magnitude of the errors none have succeeded in completely eliminating the inequilibrium of the stresses. So instead of attempting to carry out iterative corrections to the strain path calculation, a different approach has been adopted and has proved successful.

STRAIN PATH FINITE ELEMENT METHOD

The problem of cone penetration has in the past been analysed by the finite element method (DeBorst & Vermeer, 1984; Kiousis *et al.*, 1988). In these analyses the cone has effectively been introduced into a pre-bored hole with the surrounding soil still in its in-situ stress state. An incremental plastic collapse calculation is then carried out and the limit value identified as the indentation pressure. This interpretation is not entirely correct however. During the real penetration of the cone, very high lateral and vertical stresses develop adjacent to the shaft of the penetrometer. These higher soil stresses will influence the conditions around the cone tip, resulting in higher cone penetration pressures than are predicted by the analysis of the cone in a pre-bored hole. In the analysis of the cone penetration test, a careful distinction is necessary between a plastic collapse solution and a steady state penetration pressure.

In an attempt to solve the inequilibrium problem of the strain path method while still accounting for the effect of the continuous penetration, the following finite element analysis has been carried out. The method involves combining the merits of the strain path method which correctly accounts for steady state flow but results in an error in equilibrium, with the finite element

method which satisfies equilibrium correctly. This method involves using the solution from the strain path method as the initial stress condition. As stated previously these stresses are not quite in equilibrium. The inequilibrium of the initial stress state is represented as a set of out-of-balance body forces which are eliminated by applying incrementally equal and opposite forces. This correction procedure is carried out with the cone fixed. After the inequilibrium has been eliminated the cone is penetrated further until a steady load is reached. This is achieved by imposing incrementally a vertical displacement to the cone. Because of the substantial displacement involved in this operation a large strain large displacement formation of the finite element method is used.

RESULTS FROM THE STRAIN PATH METHOD

This procedure, involving the combination of the strain path method with the finite element technique, is somewhat laborious. Many results of value can be obtained purely from the strain path method (although with some concern about the equilibrium problem). In this section the results of calculations using the strain path method alone are presented.

Strain paths due to cone penetration

Cavity expansion theory has commonly been adopted in the interpretation of deep penetration problems. However, as already noted, this theory does not take into consideration the history of soil straining due to cone penetration. Therefore it does not distinguish between the different modes of soil deformation due to the different cone geometries. This limitation in cavity expansion theory may have important implications in extending it to the interpretation of the cone penetration test.

A series of strain path calculations has been carried out to study the influence of cone angle on the resultant soil strains due to cone penetration. To facilitate the interpretation of the strain history a three dimensional, orthogonal strain space described by three strain invariants E_1, E_2 and E_3 has been adopted. These strain invariants are defined as (Baligh, 1986)

$$E_1 = \varepsilon_{zz} \tag{14}$$

$$E_2 = \frac{1}{\sqrt{3}}(\varepsilon_{rr} - \varepsilon_{\theta\theta}) \tag{15}$$

$$E_3 = \frac{2}{\sqrt{3}}\gamma_{rz} \tag{16}$$

where ε_{rr}, ε_{zz}, $\varepsilon_{\theta\theta}$ and γ_{rz} are the radial, axial, circumferential and shear strains respectively. It should be noted that E_1 represents the strain mode in triaxial compression, E_2 corresponds to the strain mode in a pressuremeter test and E_3 is analogous to the strain mode in a direct shear test. The strain paths in these conventional tests can be represented in this strain space as lines along the E_1, E_2 and E_3 axes respectively.

Figure 2 shows the strain paths of soil elements located initially at a radial distance of 1·0 a from the axis of penetration, where a is the radius of the cone. The initial estimate of the flow field in these calculations was obtained by assuming that the flow of soil past the cone is similar to that of a inviscid fluid. The strain components were computed by integrating the strain rates along the line of flow from a point sufficiently far 'upstream' of the cone tip. That is

$$\varepsilon_{ij} = \int \dot{\varepsilon}_{ij}\, ds \tag{17}$$

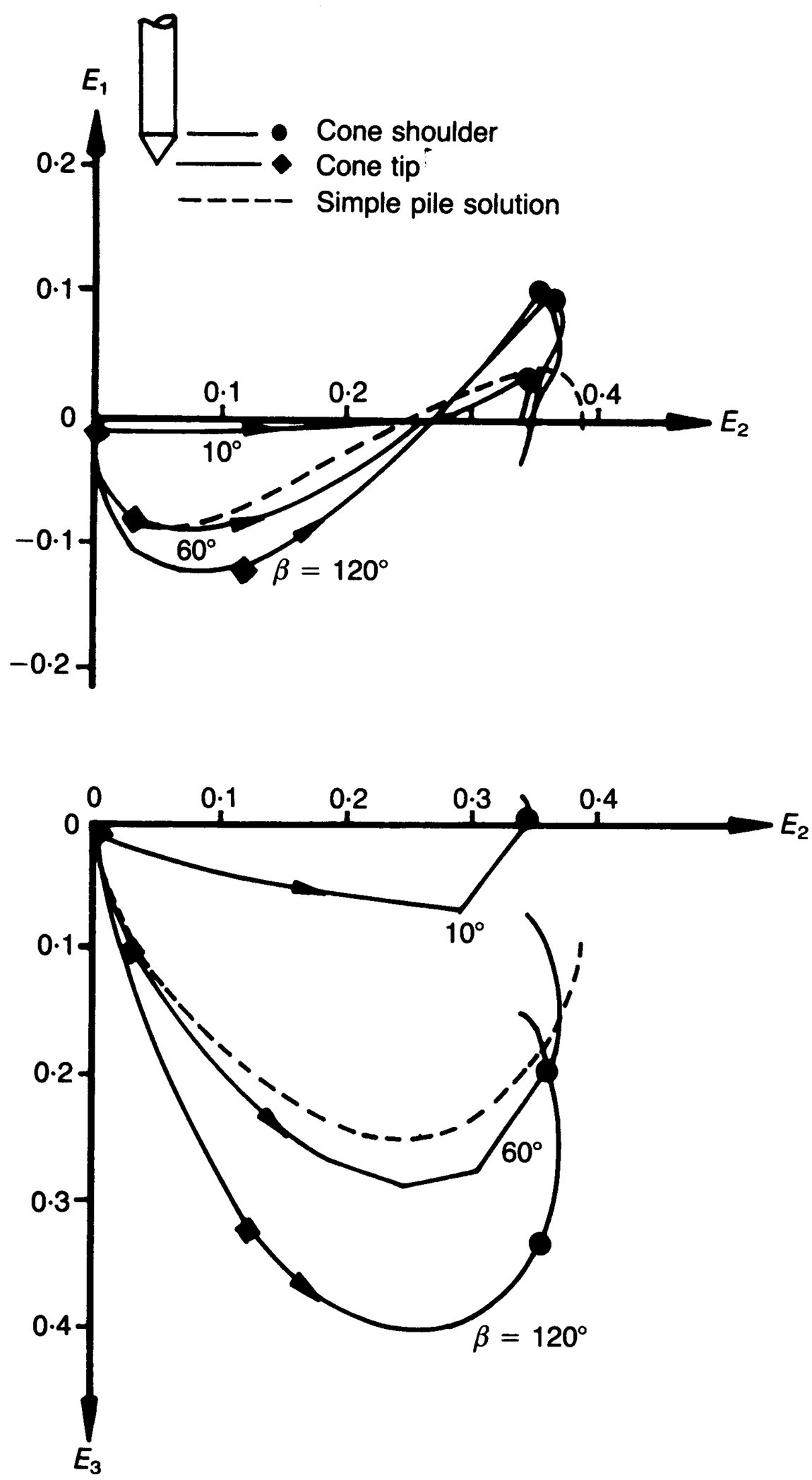

Fig. 2. Strain paths due to cone penetration

where s is measured along the line of flow. Some features of these strain paths are worthy of attention. First, irrespective of the cone angle, the magnitude of E_2 is found to reach a peak at the level of the cone shoulder. This peak value is comparable to that predicted by cylindrical cavity expansion in expanding a cylindrical cavity from zero radius to a, the radius of the shaft. A small reversal in E_2 is evident as the soil element emerges from the cone shoulder. Varying the cone angles appears to affect mainly the magnitudes of E_1 and E_3. When the cone angle is very sharp ($\beta = 10°$), E_1 and E_3 are found to be relatively small. In fact, the results shown in Fig. 2 indicate that soil deformation due to the penetration of a very sharp cone is comparable to that predicted by cavity expansion theory. This result is consistent with the findings of Norbury & Wheeler (1987) who provided an analytical solution to the steady penetration of a slender body. Their analysis showed that in the limiting case of the penetration of a very slender penetrometer into a infinite elastic perfectly plastic continuum, the deformation field was similar to the solution obtained from cylindrical cavity expansion theory.

Increasing the cone angle results in a significant increase in both E_1 and E_3. Below the cone tip the axial soil strains are predominantly compressive but as the soil moves past the conical section of the penetrometer the axial strain reverses its sign, reaching a peak tensile value at about the cone shoulder level. Beyond the cone shoulder the magnitude of E_1 gradually decreases to a value close to zero.

For the purpose of comparison the strain path caused by the penetration of a simple pile (as defined by Baligh, 1986) has also been plotted in Fig. 2. The general trend of variation of E_1 and E_3 for a simple pile is broadly similar to that of the cone penetrometer. One notable difference is in the E_2 strain component. For cone penetration reversal in E_2 is evident as the soil emerges from the cone tip region. In the case of a simple pile E_2 increases monotonically without any reversal. Hence, it seems reasonable to associate the reversal in E_2 to the geometry of the cone.

The contours of the soil strain components ε_{rr} and ε_{zz} around a standard 60° cone are shown in Fig. 3. It is interesting to note that below the tip the strain contours are broadly similar to those predicted by spherical cavity expansion theory. In addition, the variation of soil strains with radial distance at a level far away from the tip is qualitatively similar to the cylindrical cavity expansion solution. In the vicinity of the cone, however, the soil strain distribution is too complex to be approximated by either of these idealized solutions. Since most of the sensing instruments are located at or near the cone tip region in a conventional penetrometer design, it would appear from the complex soil deformation that exists around the cone that cavity expansion theories do not provide a sufficiently rigorous basis for the interpretation of cone data.

It is a common practice in assessing the level of

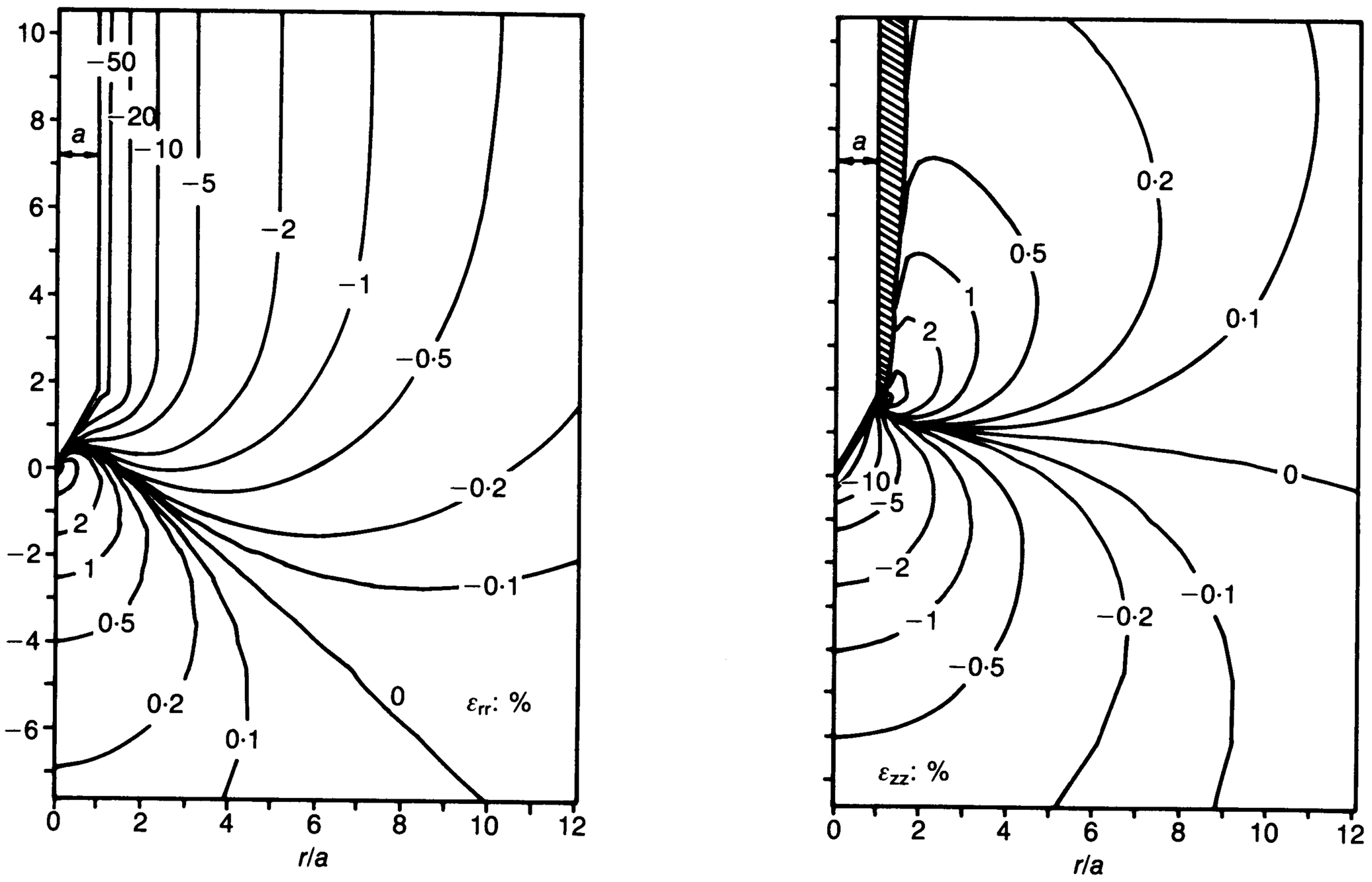

Fig. 3. Radial and axial strain contours around a 60° penetrometer

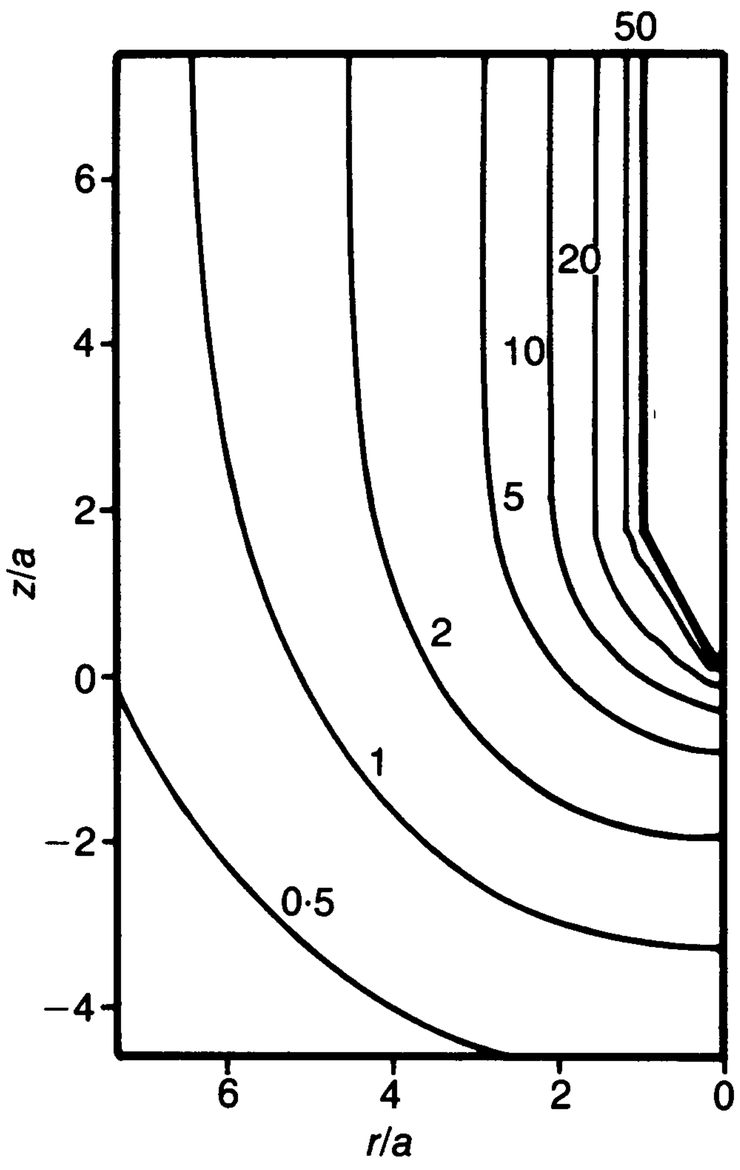

Fig. 4. Contours of γ_{oct}(%) around a 60° cone penetrometer

straining to evaluate the octahedral shear strain, which is defined as

$$\gamma_{oct} = \frac{1}{\sqrt{2}} [E_1^2 + E_2^2 + E_3^2]^{1/2} \qquad (18)$$

The contours of γ_{oct} for a 60° cone are shown in Fig. 4. The results show a region of very high soil strain in the immediate vicinity of the penetrometer. It is of interest to note that for an elastic–perfectly plastic material, the elastic–plastic boundary coincides with one of the γ_{oct} contours. The value of γ_{oct} at which yielding of soil occurs is dependent on the ratio of G/s_u. The location of this boundary for different soil properties will be addressed in a later section.

Stress changes due to cone penetration

Once the deformation history of the soil element has been evaluated, it is a relatively straightforward matter to compute the deviatoric stresses. The calculation process is carried out by tracking an individual soil element as it flows around the cone. By monitoring the changes in the soil strain as the soil element traverses a small distance along the 'streamline,' the stress changes can be computed using the appropriate incremental equation (equations (4) to (7) together with the yield criterion, equation (1)). By repeating this process along a sufficiently large number of streamlines, the pattern of the soil stress around the penetrometer can be built up. In the case in question the computation was carried out using a finite difference scheme.

Since the strain paths due to sharp cone penetration are quite similar to those due to cylindrical cavity expansion there is good reason to believe that the stress changes in the two cases may also be similar. This has indeed been found to be the case. Fig. 5 shows the variation of the total stress components with radial distance for a penetrometer with a 10° cone angle (the calculation of the mean pressure component is discussed in the following section). The stresses were computed by adopting a von Mises yield criterion and a rigidly index I_r of 100. The result derived from cylindrical expansion theory (Sagaseta, 1985) for the same set of material parameters is also shown in the plot. There is good agreement between the stresses obtained from the two

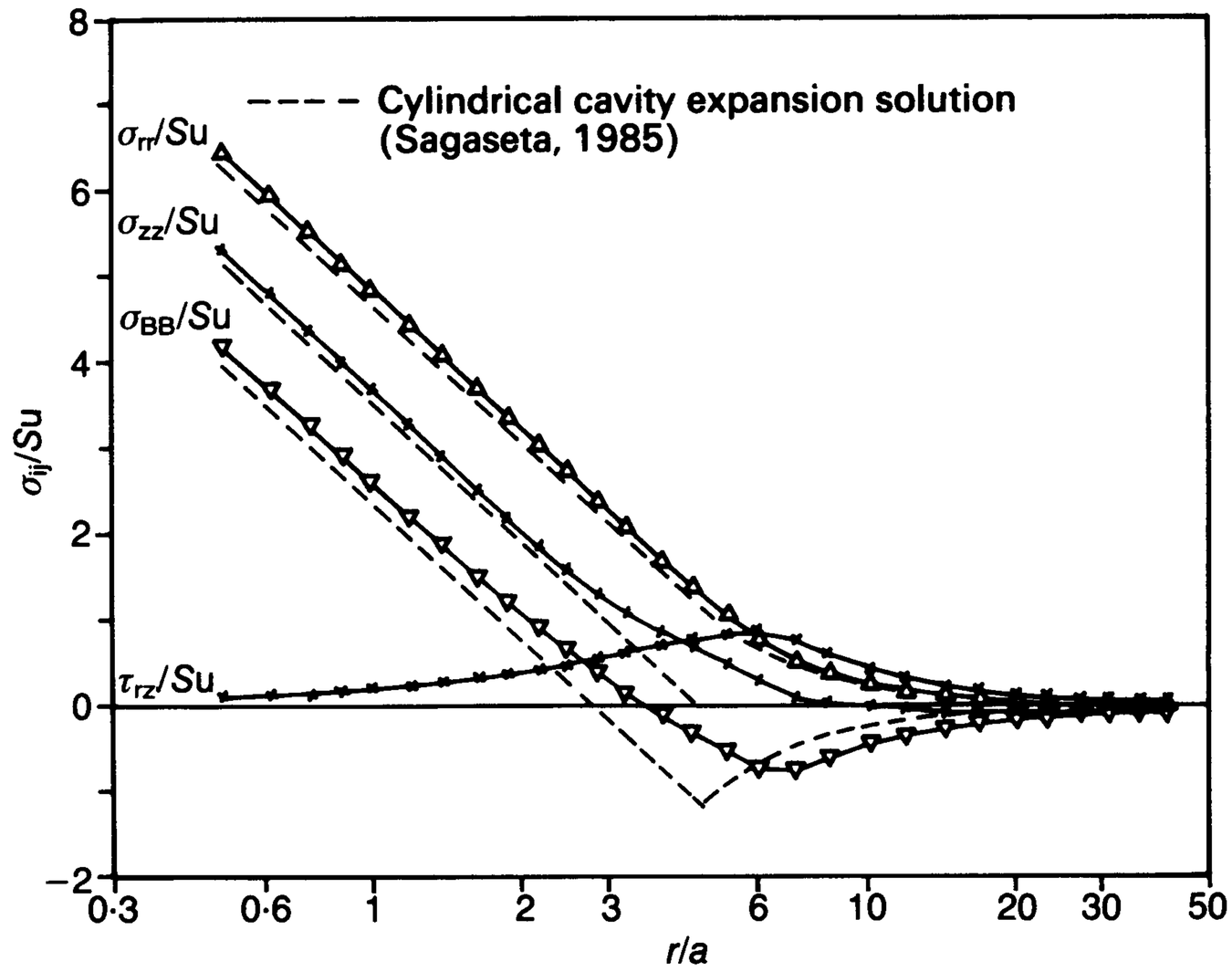

Fig. 5. Variation of stresses with radial distance on a horizontal plane at mid cone (β − 10° I_r − 100)

methods of solution except in the shear stress component. While cavity theory predicts zero shear stresses due to the plane strain nature of the problem, sharp cone penetration results in small finite shear stresses. The maximum deviation between the two solutions occurs near the elastic–plastic boundary. This small discrepancy may be due in part to the discrete nature of the numerical solution.

Mean pressure calculation

Based on the computed deviatoric stresses the mean pressure may be calculated using the equilibrium equations. In principle either of the equilibrium equations can be used for this purpose. For a set of deviatoric stresses in equilibrium the mean pressure computed using one of these equations will satisfy the other equation. This however, is not true if the stresses are only approximate. Alternatively the two equilibrium equations may be combined into a single Poisson's equation. The solution to this equation can be considered to satisfy each equilibrium equation approximately if the appropriate boundary conditions are adopted.

The mean pressure obtained from the integration of the equilibrium equation in the radial direction p_r is shown in Fig. 6(a). It is believed that this provides a better solution to the mean normal stresses than the solution obtained by integrating the equilibrium equation in the axial direction. This is supported by the solution of the Poisson equation shown as p_p in Fig. 6(b). The good agreement of the solutions obtained from two different methods provides evidence of the reliability of the mean pressure solution. In particular the computed soil stresses around the cone tip region are nearly identical. The cone resistance values derived from these two solutions differ by less than 5%.

Extent of the failure zone due to cone penetration

Cone penetration causes a zone of soil around the penetrometer to deform plastically. The failure zone around a penetrometer may be described by the elastic–plastic boundary which divides the soil into an elastically deforming region and a plastically deforming region. The extent of this failure zone is dependent on several factors, chief among which are the shear strength of clay s_u and its shear modulus G. Cavity expansion theory predicts that the elasto-plastic radius is related to these two soil parameters via a single dimensionless factor I_r. For the cone penetration problem, the plastic boundary may be characterized by two parameters, r_p and z_p (Fig. 7), where r_p is the radial distance of the plastic boundary from the axis of penetration measured at a large enough distance above the cone tip, and z_p is the distance between the cone tip and the boundary measured along the axis of the penetrometer.

The variations of r_p and z_p with I_r are shown in Fig. 7. The normalized plastic radius r_p is found to be independent of the cone angle. The magnitude of z_p on the other hand is affected significantly by changes in cone angles. For a cone angle of 10° and I_r of less than about 100, z_p is zero, indicating that the plastic boundary intersects the cone tip. This implies that the soil adjacent to the cone tip may be divided into a plastic

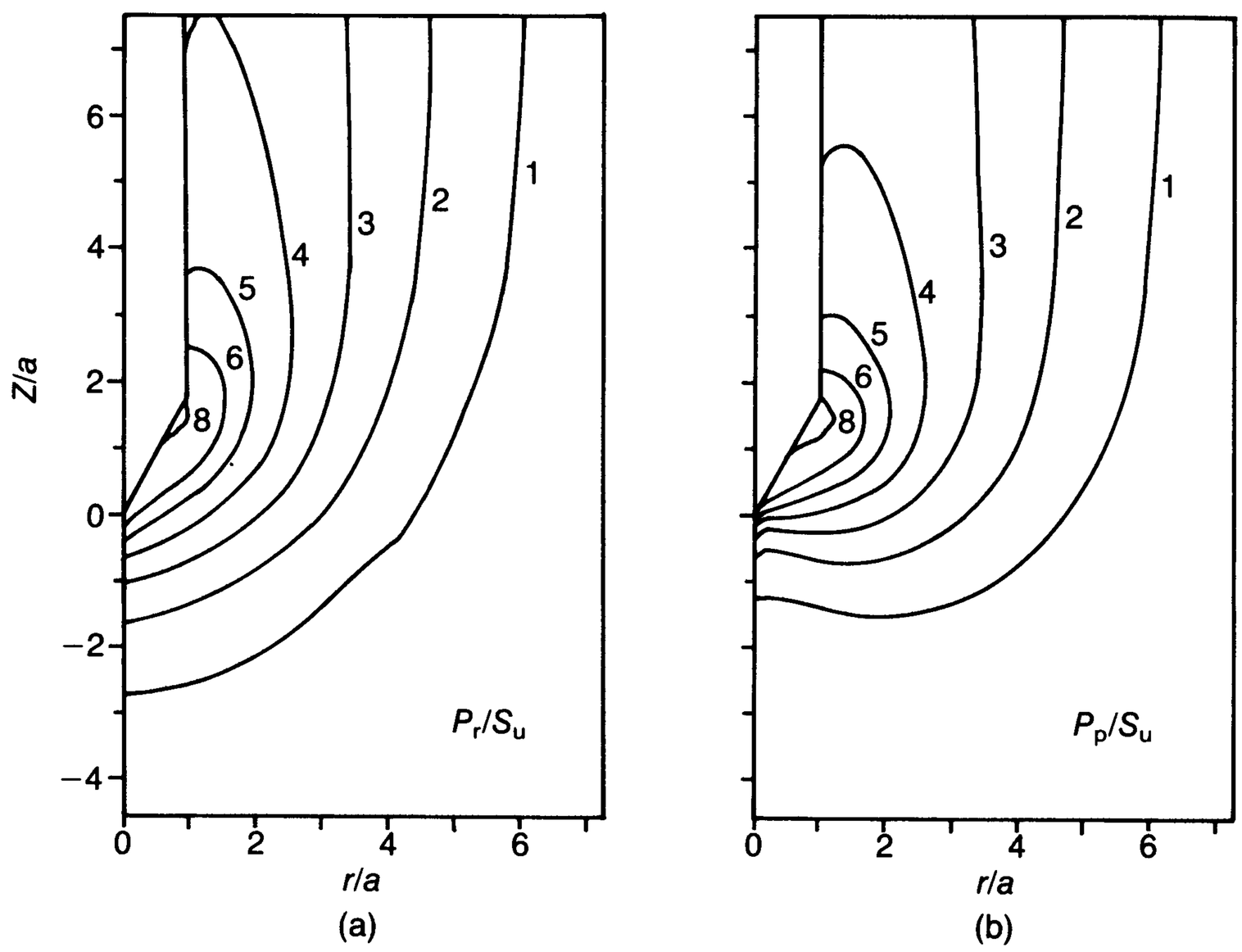

Fig. 6. Normalized mean pressure contour evaluated using (a) radial equilibrium equation and (b) Poisson's equation

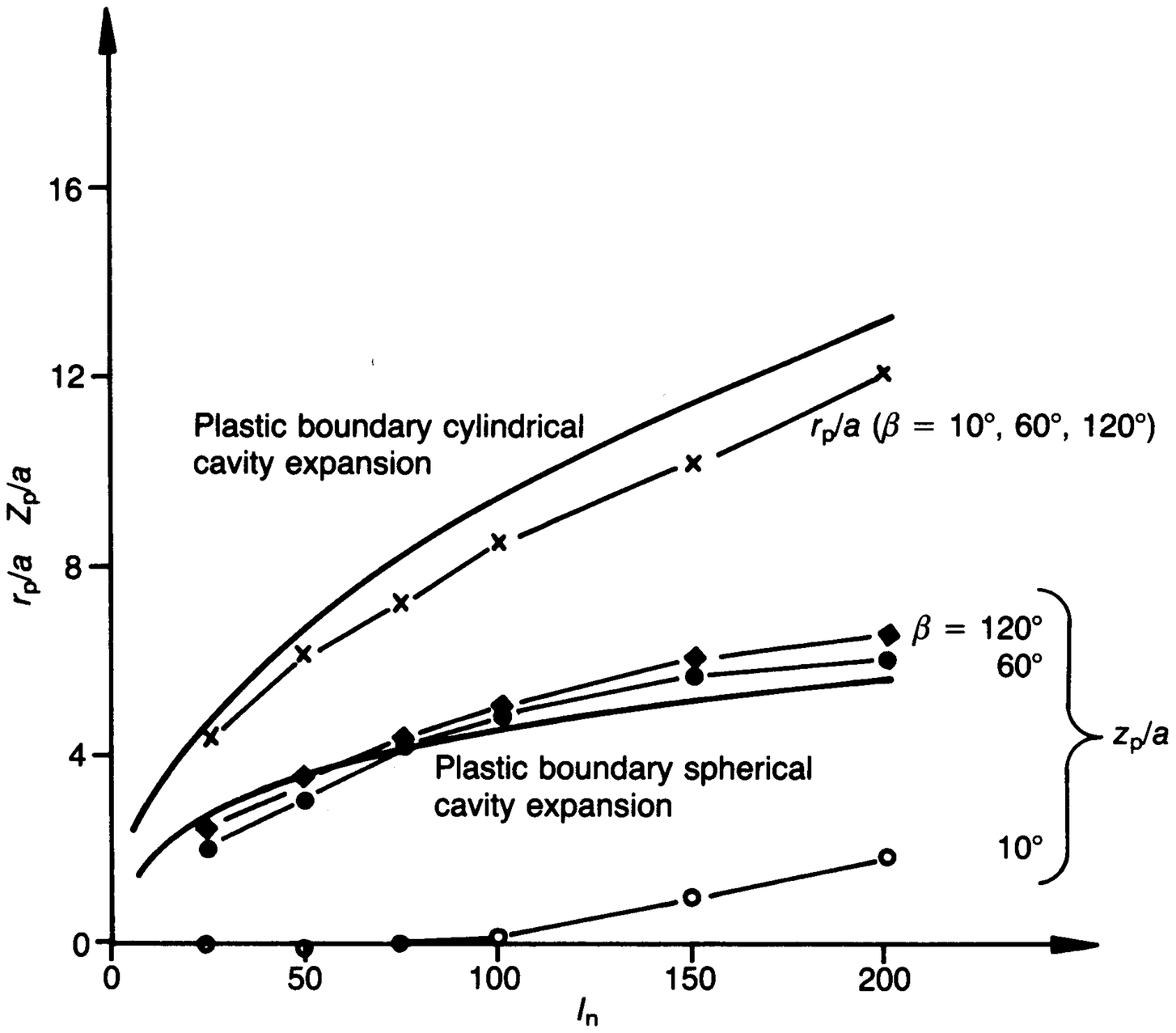

Fig. 7. Location of the elasto-plastic boundary in cone penetration

and an elastic zone. This is different from the deformation mechanism associated with the penetration of a penetrometer with a more obtuse cone angle. Thus, for the combination of a very sharp cone angle and low I_r, the cone can be said to cut through the soil. In other cases the penetration process causes compressive plastic yielding of the soil ahead of the penetrometer (Fig. 8). Similar findings have been obtained by Sagaseta & Houlsby (1988) who studied the problem around the tip of an infinite cone.

For cone angles of 60° and 120° the values of z_p are comparable to the spherical cavity expansion solution. While the agreement is due partly to the arbitrary choice of the tip as the datum for measuring z_p, it is nevertheless significant that for this range of cone angles the trend of variation of z_p with I_r agrees closely with the spherical cavity expansion solution.

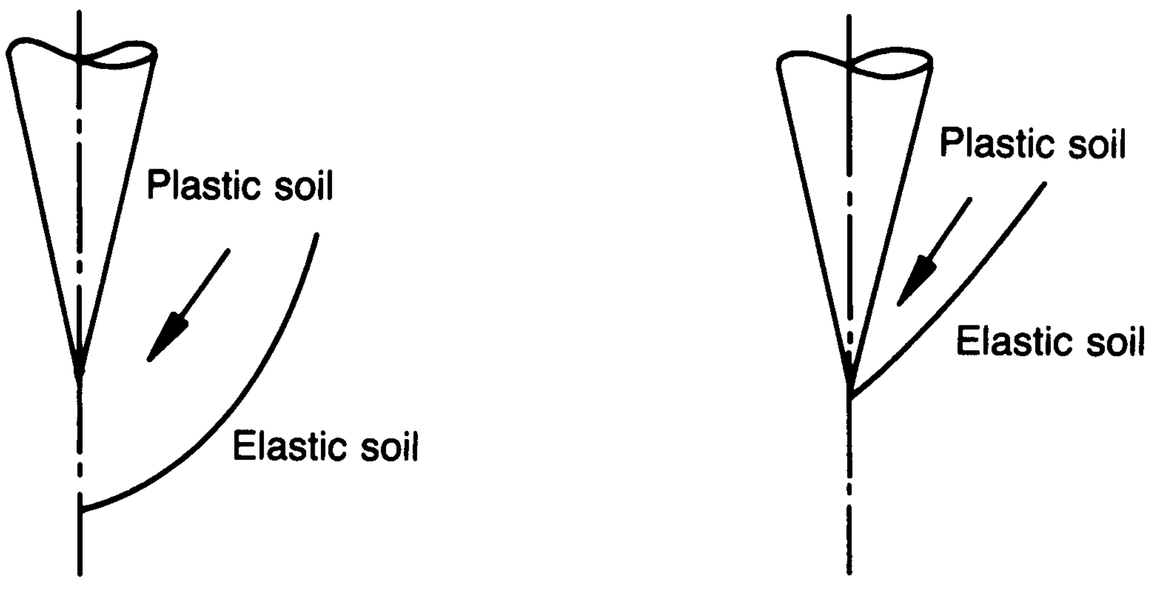

Fig. 8. Possible soil states around penetrometer tip

Cone factor from strain path solution

Having computed the total soil stresses around the cone the tip resistance q_t is evaluated by integrating the relevant stress components over the cone face. The results for a 60° cone in clays of different rigidity indices are shown in Fig. 9. The initial soil stresses are assumed to be isotropic. The tip resistance has been plotted as a normalized cone factor N_{kt} where

$$N_{kt} = \frac{q_t - \sigma_{vo}}{s_u} \tag{19}$$

and σ_{vo} is the in-situ vertical stress. The limit pressure for the expansion of a cylindrical and a spherical cavity are similarly normalized by replacing q_t in equation (19) by Ψ_c and Ψ_s respectively. The magnitude of N_{kt} for a 60° cone derived from the strain path method is higher than the cavity expansion solutions and can be approximated by the expression

$$N_{kt} = 1{\cdot}25 + 1{\cdot}84 \ln (I_r) \tag{20}$$

In carrying out these calculations no control of the shear stress boundary condition on either the cone face or the shaft is possible. The results are found to correspond to a cone roughness factor α_f of approximately zero where

$$\alpha_f = \frac{\sqrt{(3)}\tau_f}{2s_u} \tag{21}$$

$0 < \alpha_f < 1$ and τ_f is the shear stress on the cone face boundary. If roughness variation is assumed

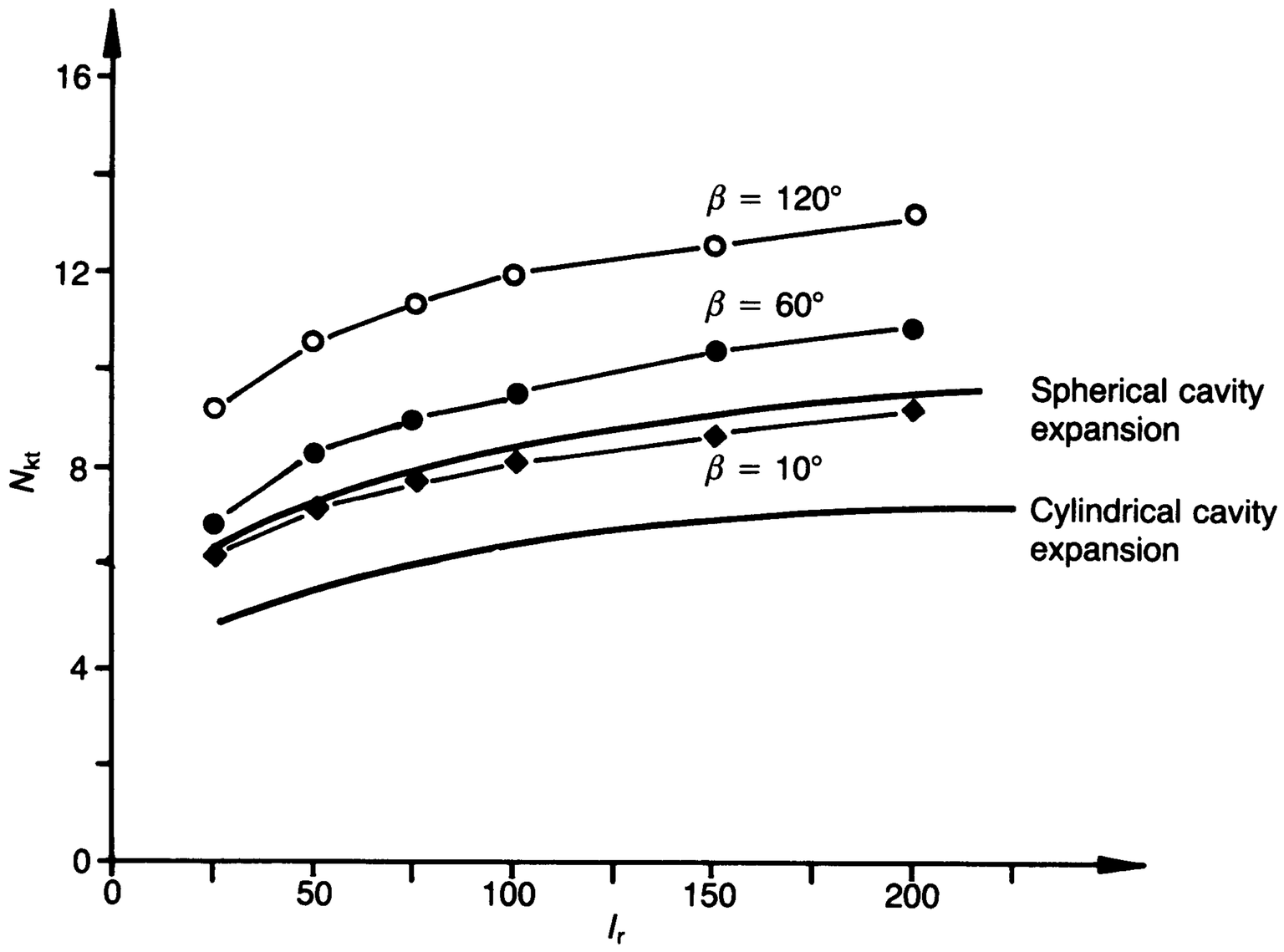

Fig. 9. Variation of N_{kt} with I_r based on strain path method

to have no significant effect on normal stress distribution on the face of the cone, then it can be accounted for entirely by considering the additional vertical force component due to the shear stress. This results in an additional term equal to

$$\frac{2\alpha_f}{\sqrt{(3)}\tan(\beta/2)} \tag{22}$$

where β is the cone angle. For the conventional 60° cone this reduces to $2\alpha_f$ so that equation (19) becomes modified to

$$N_{kt} = 1{\cdot}25 + 1{\cdot}84 \ln(I_r) + 2\alpha_f \tag{23}$$

Effect of in-situ soil stresses

In a natural clay deposit the in-situ horizontal stress is usually different from the vertical stress. The effect of initial stress anisotropy on cone resistance is investigated by varying the in-situ horizontal and vertical stresses. The stress distributions due to the penetration of a 60° cone for two sets of initial stress conditions are shown in Fig. 10. The soil is assumed to have an I_r of 100. The initial stresses for the two cases are

$$\frac{\sigma_{ho}}{s_u} = 2{\cdot}0, \qquad \frac{\sigma_{vo}}{s_u} = 3{\cdot}5 \tag{24}$$

for case (a) and

$$\frac{\sigma_{ho}}{s_u} = 3{\cdot}5, \qquad \frac{\sigma_{vo}}{s_u} = 2{\cdot}0 \tag{25}$$

for case (b) where σ_{ho} is the in-situ horizontal stress. Fig. 10 shows that in both cases the radial

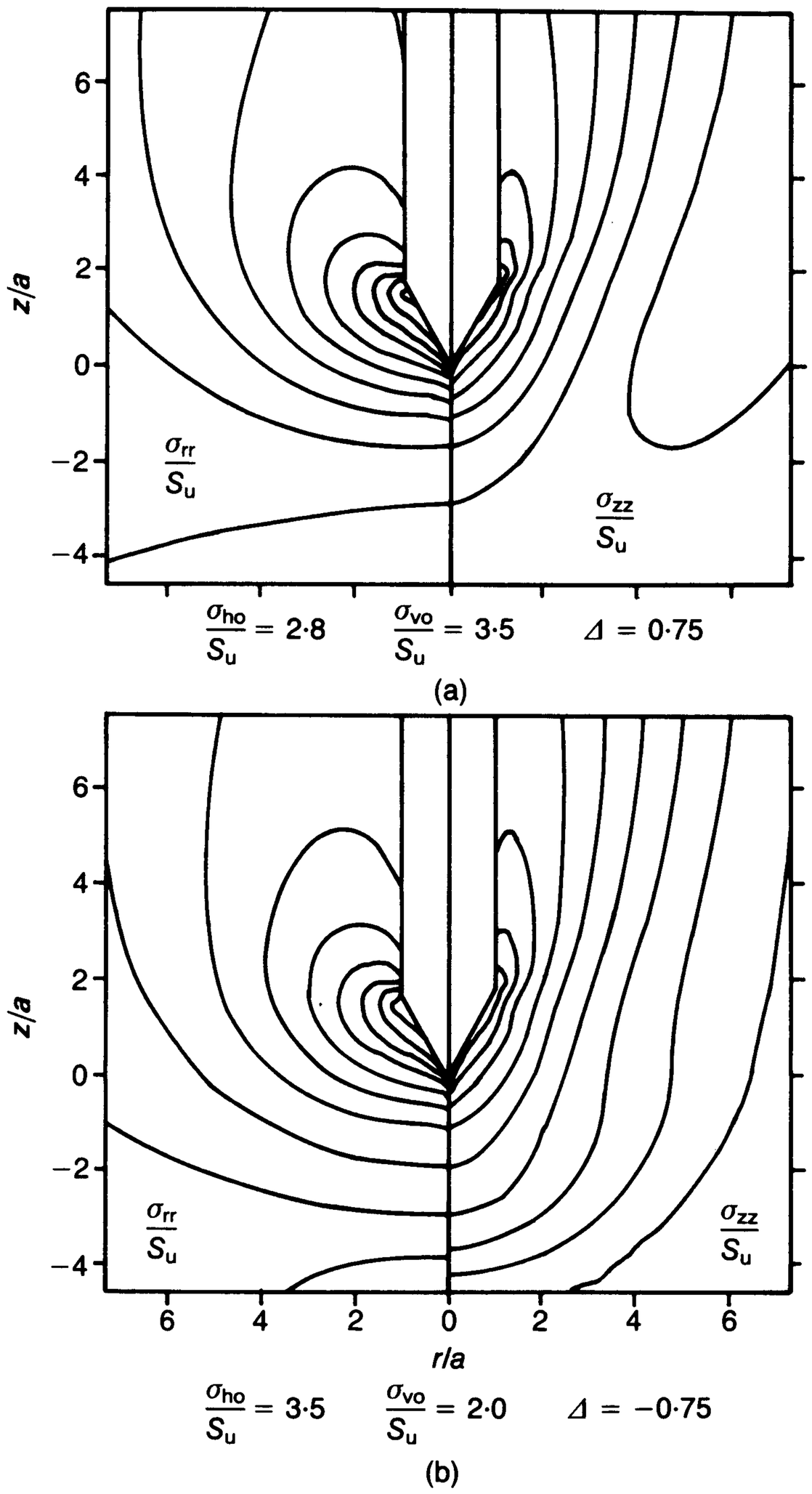

Fig. 10. Normalized stress contours for different initial stress states (β = 60°)

stress distributions are very similar. However, the axial stress in case (b) is considerably higher despite the fact that the initial vertical stress is lower. This higher axial stress component in case (b) leads to higher computed cone factor N_{kt}. The calculation has been repeated for other combinations of initial stresses. For convenience of presentation, the initial stress conditions are characterized by a dimensionless factor Δ, defined as

$$\Delta = \frac{\sigma_{vo} - \sigma_{ho}}{2s_u} \tag{26}$$

The possible values of Δ are in the range $-1 \leqslant \Delta \leqslant 1$. The variation of N_{kt} with Δ is shown in Fig. 11. The results fall very close to a line of slope -2 on this plot. This suggests that it is more consistent to define the cone factor in terms of the horizontal stress in a relationship such as

$$N_h = \frac{q_t - \sigma_{ho}}{s_u} \tag{27}$$

rather than equation (18). However, since σ_{ho} is not usually known accurately, it would be more practicable to retain the use of the N_{kt} factor, but due recognition must be paid to the effect of the horizontal stress by further modifying equation (21) to

$$N_{kt} = 1{\cdot}25 + 1{\cdot}84 \ln (I_r) + 2\alpha_f - 2\Delta \tag{28}$$

While this approximate solution is of value there remains a doubt about the significance of the inequilibrium of the stress. In order to resolve this problem the results of the alternative series of calculations, which combines the strain path method with the finite element technique must be used.

Results of strain path finite element analysis

Instead of attempting to carry out iterative corrections of the strain path calculation which proved not to be completely successful (see Appendix 1), a different approach has been adopted to address the inequilibrium problem. The method involves combining the merits of the strain path method, which correctly accounts for steady flow but results in an error in equilibrium, with the finite element method which satisfies the equilibrium requirement.

As already described, the solution algorithm begins with the penetrometer being held stationary while the out-of-balance forces are eliminated by incrementally applying equal and opposite forces. After the inequilibrium has been eliminated in this way the cone is pushed down further by prescribing incremental displacement to the penetrometer until a steady load is reached. Due to the incompressibility condition which must be satisfied, a finite element mesh consisting of fifteen-noded triangular elements has been adopted to ensure a correct limiting solution (Sloan & Randolph, 1982). The incompressibility condition is approximated by using a Poisson's ratio of 0·49 in all the calculations. A typical finite element mesh is shown in Fig. 12.

It has been observed that if the out-of-balance body forces are not too large then the first stage of the analysis involving the inequilibrium correction is not strictly necessary. With the modified

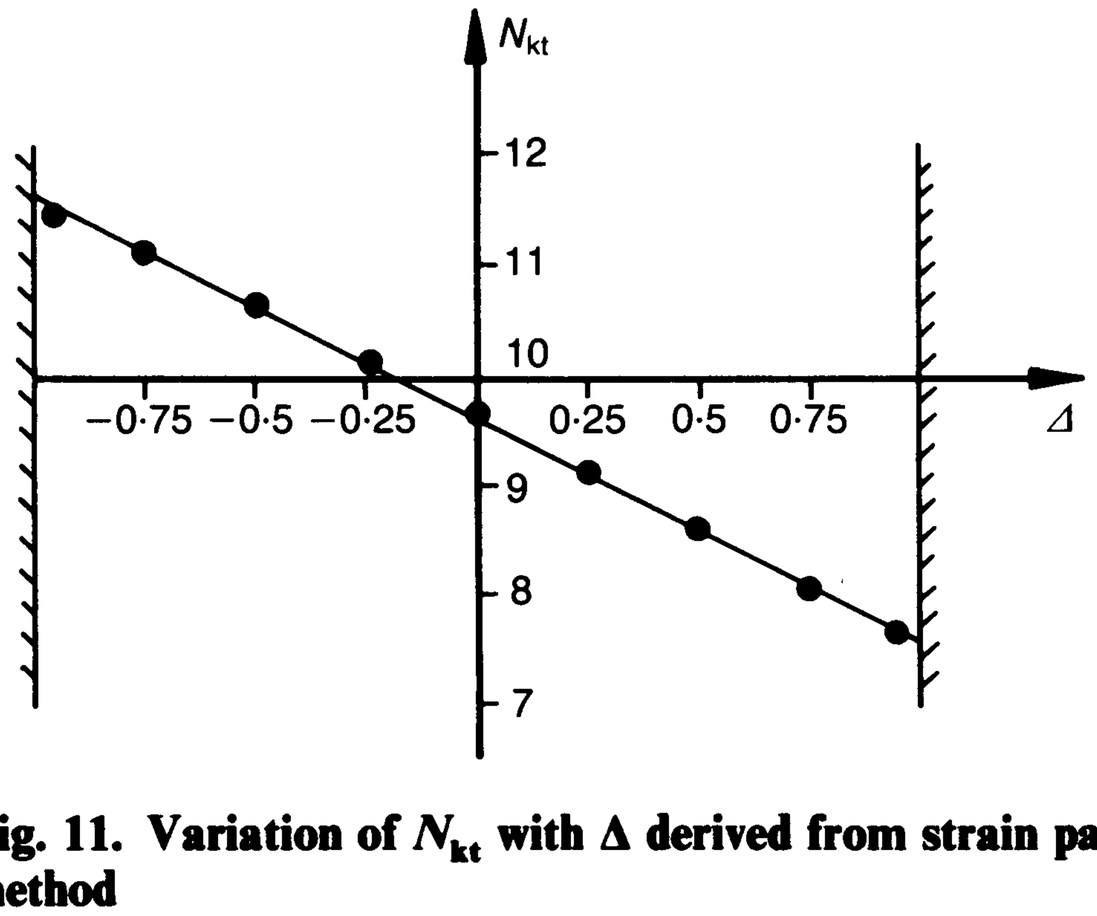

Fig. 11. Variation of N_{kt} with Δ derived from strain path method

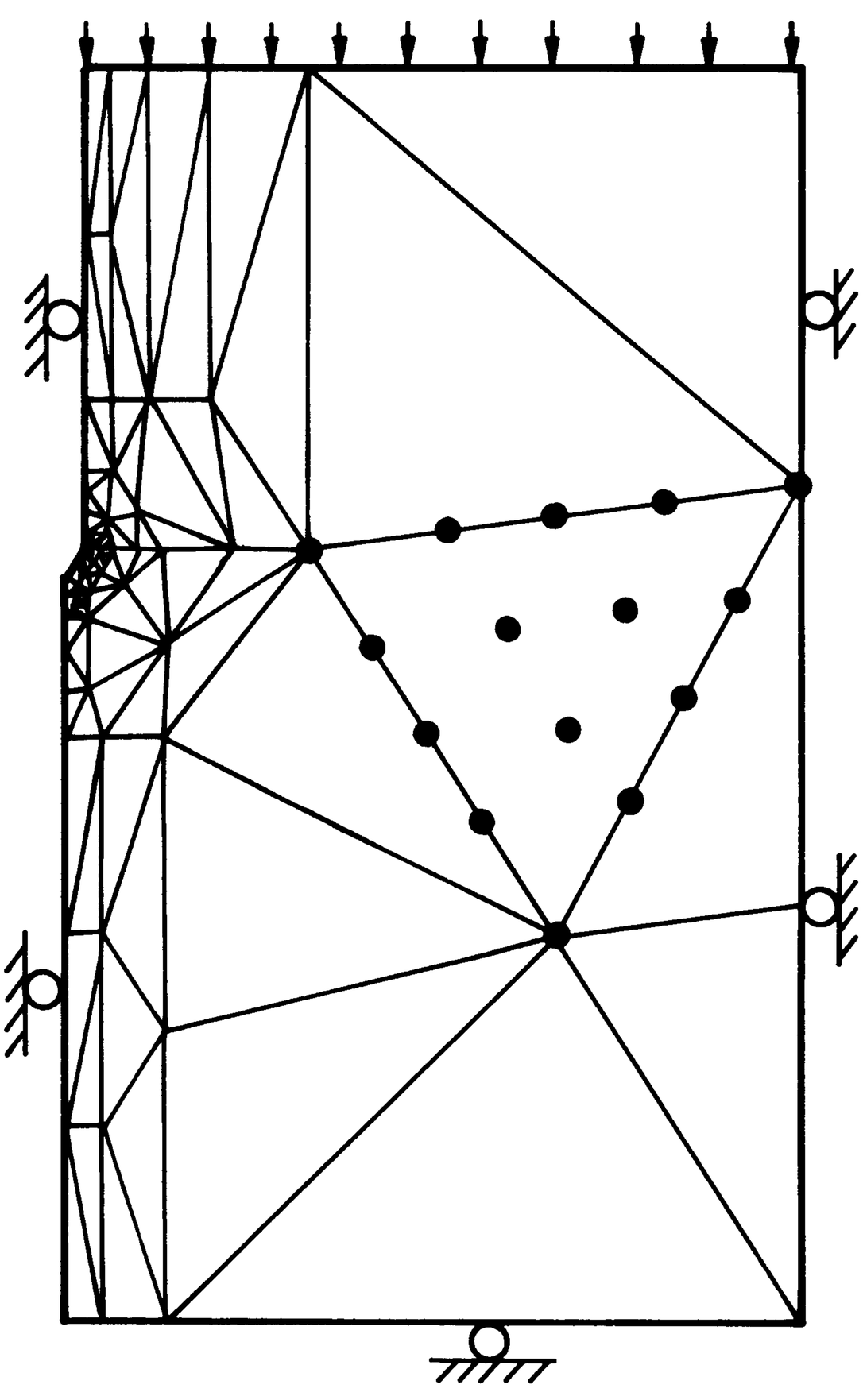

Fig. 12. Fifteen-noded finite element mesh

Euler solution scheme (Teh, 1987) used in the finite element algorithm, the errors of equilibrium in the stresses at the beginning of each incremental stage are automatically evaluated. The out-of-balance stresses are then treated as residuals to be imposed as an additional load in the next load increment. Therefore, if the initial stresses are only out of equilibrium by a small amount, then the error can easily be handled by the inherent correcting mechanism in the solution algorithm. This has been verified in a series of calculations in which the initial inequilibrium correction is not performed.

Figure 13 shows a comparison of three analyses using the finite element method in which the cone resistance expressed as N_{kt} is plotted against penetration. A rigidity index of 100 is assumed in the calculation. Curve A is a conventional analysis starting from the in-situ stress state which is assumed to be isotropic; curve B is an analysis as described above with a preliminary correction of the out-of-balance body forces; and curve C represents a similar analysis but without the preliminary equilibrium correction calculation. The same in-situ stress state has been adopted for the conventional finite element calculation (curve A) and the strain path calculations preceding the finite element analysis for the two latter cases (curves B and C) to provide a consistent framework for comparison.

From Fig. 13, it is apparent that conventional finite element calculation results in a smaller cone factor. The limiting N_{kt} value of 10·23 is comparable to the results of previous works (DeBorst & Vermeer, 1984; Kiousis *et al.*, 1988). This figure does not, however, represent the conditions around the cone accurately. The initial equilibrium correction has a negligible effect on the

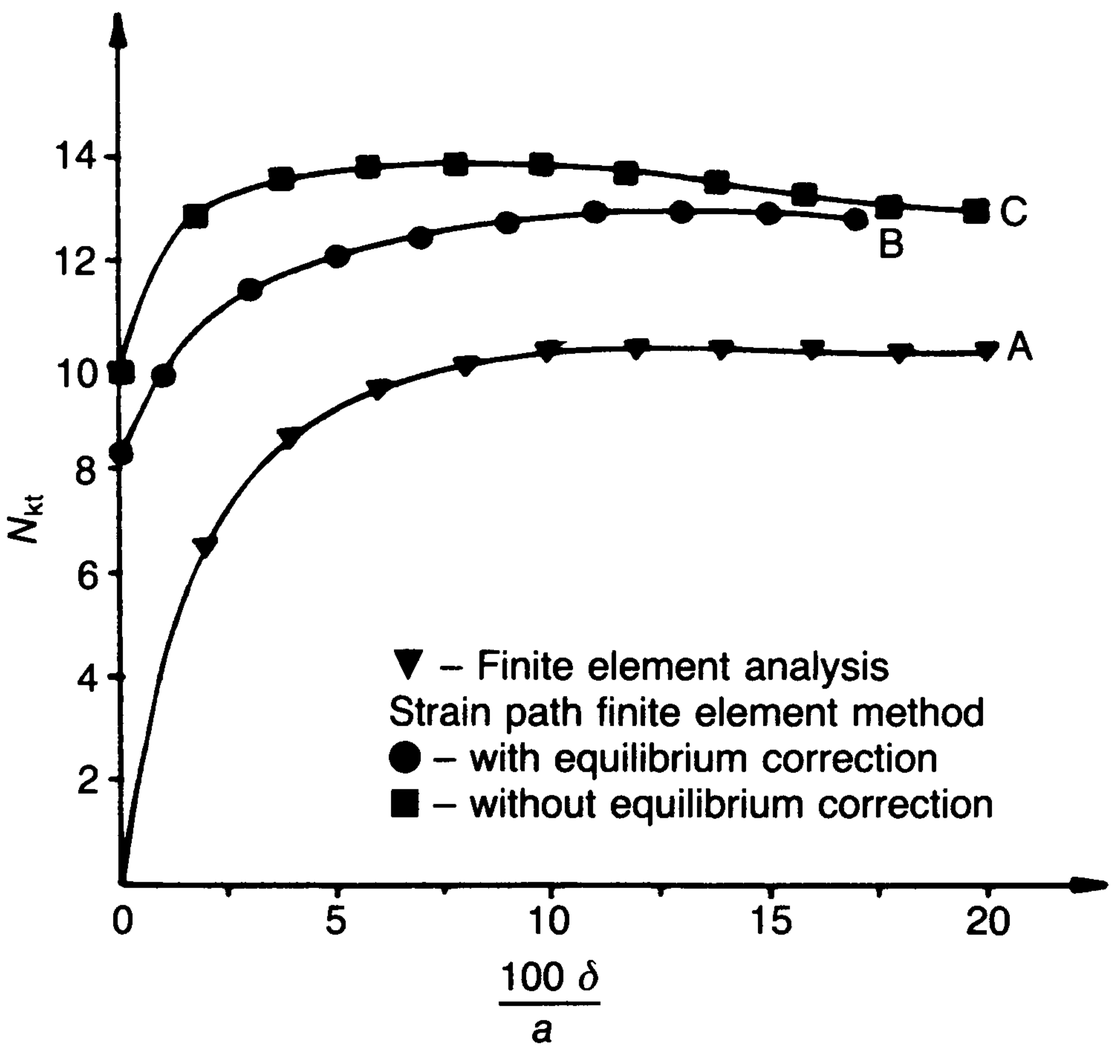

Fig. 13. Variation of N_{kt} with cone displacements

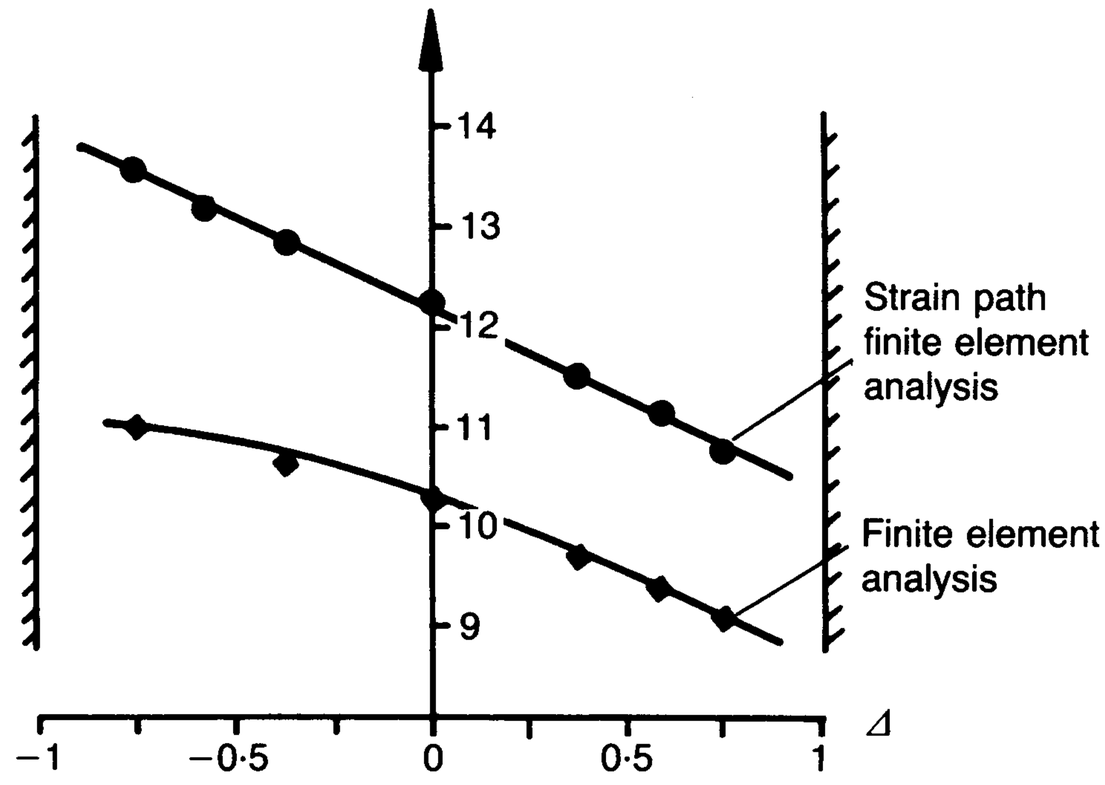

Fig. 14. Variation of N_{kt} with Δ derived from finite element calculations

ultimate cone resistance obtained from strain path finite element calculations. The limiting cone factors from the two analyses are found to differ by less than 1%. The limiting value of N_{kt} based on curve C is found to be 13·08, which is 28% higher than the 10·23 calculated using the inappropriate initial stresses.

For different combinations of initial horizontal and vertical stresses, the variation of N_{kt} with Δ obtained by the strain path finite element method is as shown in Fig. 14. The slope of the best straight line fitting the computed data has a slope of approximately −1·8, as opposed to −2·0 as obtained with strain path calculations. Interestingly, the effect of horizontal stress variation on cone factor N_{kt} is also apparent in the conventional finite element calculations.

In an attempt to assess the effect of shaft friction on the cone penetration problem conventional finite element analyses (for the pre-bored case) have been made of cones with smooth and rough shafts. The cone face in all the calculations was assumed to be rough (an unfortunate necessity conditioned by the finite element program available). The results of these calculations are presented in Fig. 15. The cone on a rough shaft is found to have a slightly lower tip resistance because part of the vertical load is carried by friction on the shaft. Although it is difficult to quantify the results from these analyses the trend of influence of shaft roughness is consistent with previous work by Houlsby & Wroth (1982). These workers obtained more quantitative information on the effect of cone and shaft roughness from a study of cones near the surface of a clay using the method of characteristics. Their results indicated that surface roughness causes a slight increase in mean stress on the cone face, suggesting a factor of $2{\cdot}4\alpha_f$ rather than the $2\alpha_f$ in equation (28). The reduction due to shaft roughness factor α_s (defined similarly to α_f) can be approximated by a further term of $-0{\cdot}2\alpha_s$.

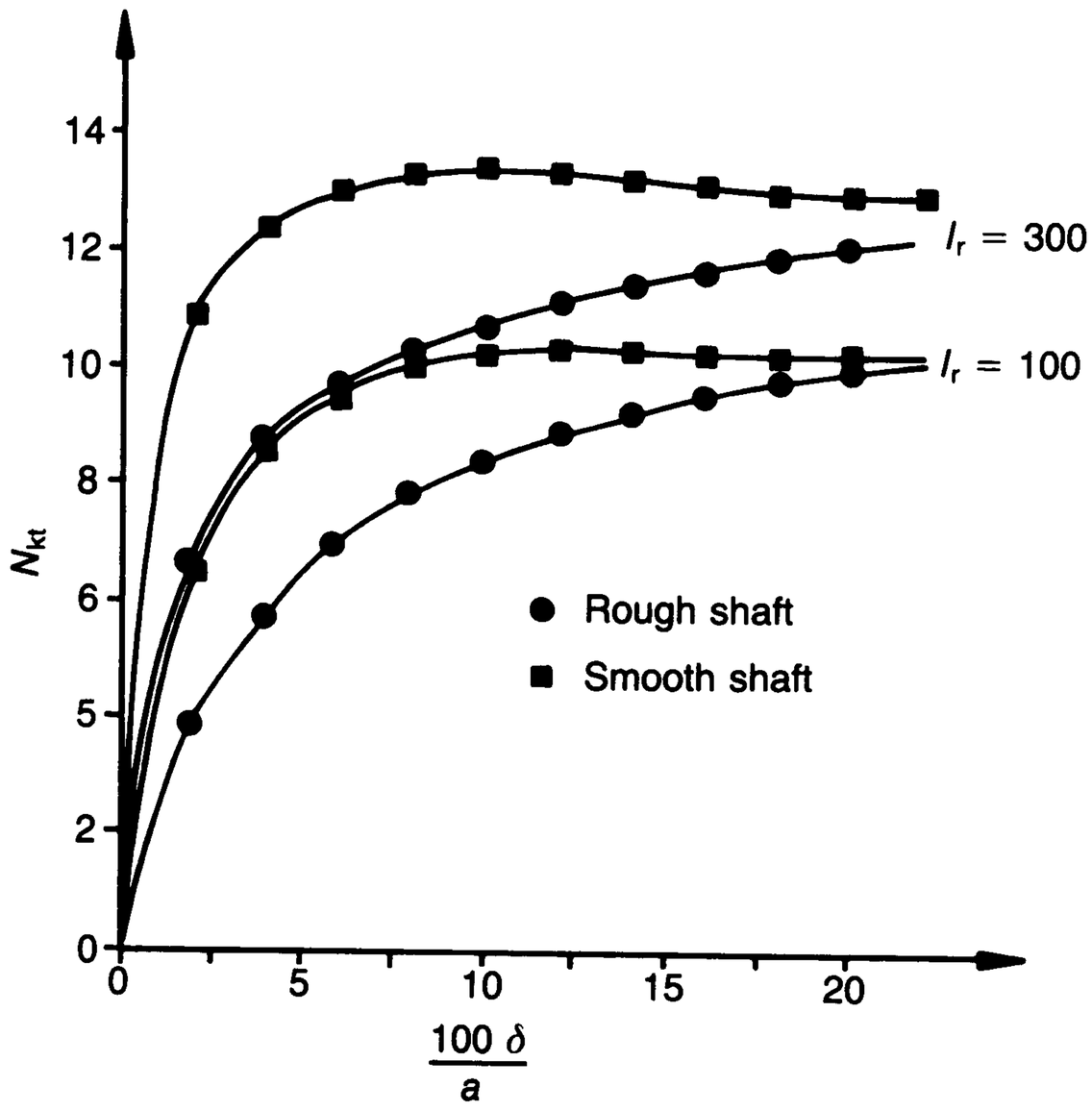

Fig. 15. Effect of shaft roughness on cone factor N_{kt}

Strain path finite element analyses do not result in precisely linear variation of N_{kt} with ln (I_r) as obtained from cavity expression theory. Correlating the results of all calculations it has been found that they can be very satisfactorily fitted by applying a simple factor to the solution for spherical cavity expansion. The final result is an approximate expression for N_{kt} which includes the effect of rigidity index, cone roughness and in-situ stresses

$$N_{kt} = N_s\left(1{\cdot}25 + \frac{I_r}{2000}\right) + 2{\cdot}4\alpha_f - 0{\cdot}2\alpha_s - 1{\cdot}8\Delta \qquad (29)$$

where N_s is the factor which appears in the spherical cavity expansion expression, that is

$$N_s = \tfrac{4}{3}[1 + \ln (I_r)] \qquad (30)$$

Equation (29) applies for the range of soil and cone parameters shown in Table 1. In extreme combinations equation (29) results in an N_{kt} factor which ranges from 6·4 to 18·6, but for more typical cases gives N_{kt} factors in the range 9 to 17. Although it is not possible to test the full range of roughness cases this expression approximates the finite element calculations (13 runs) to better than 2% in every case. Note that equation (29) requires estimates of rigidity index and the in-situ horizontal stress (as well as cone roughness) to be made before q_t can be used to estimate s_u. The derived value of s_u may then be used to refine the estimate of I_r. While this procedure may be cumbersome, it is unavoidable if the influence of stiffness on N_{kt} is to be accounted for.

Table 1. Applicable range of soil and cone parameters

Parameters	Valid range
I_r	50 to 500
Δ	−1 to 1
α_f	0 to 1
α_s	0 to 1

Since this analysis properly accounts for the high stresses developed on the cone shaft during penetration, it results in higher cone factors than have previously been derived theoretically. The higher cone factors are closer to those observed in practice. It is therefore believed that the analysis provides a reasonable solution to the cone penetration problem.

CONSOLIDATION ANALYSIS

The simultaneous measurement of pore pressure and tip resistance in a cone penetration test is gaining popularity. The additional information on the excess pore pressure provides an excellent means of determining soil stratification. There have been suggestions (Torstensson, 1977; Baligh & Levadoux, 1985) that the dissipation of pore pressure after stopping the penetration process can yield valuable information on the hydraulic properties of the clay, such as the permeability and consolidation coefficient.

The pore pressure developed during cone penetration can be expressed in terms of the change of mean normal soil stress and octahedral shear stress by the approximate relationship (Henkel, 1959)

$$\Delta u = \Delta\sigma_{oct} + \alpha\Delta\tau_{oct} \qquad (31)$$

The contribution to the total pore pressure change from the $\Delta\tau_{oct}$ term in equation (31) is relatively small and excess pore pressure changes are primarily due to changes in the mean stress. The effect of the pore water parameter α is therefore small and, for convenience, a value of $\alpha = 1{\cdot}0$ (which would be relevant, for instance, for a normally consolidated clay) has been used in this study.

In order to ensure a meaningful dissipation analysis the reliability of the predicted excess pore pressure distribution must be verified. Unfortunately, good records of pore pressure distribution in soil are rare. An exceptional case of such a pore pressure record during deep penetration is provided by Roy *et al.* (1981) who conducted a series of pile tests in St Alban clay. Prior to the tests piezometers were installed at various radial distances and at different depths in the soil around the axis of penetration of the test pile.

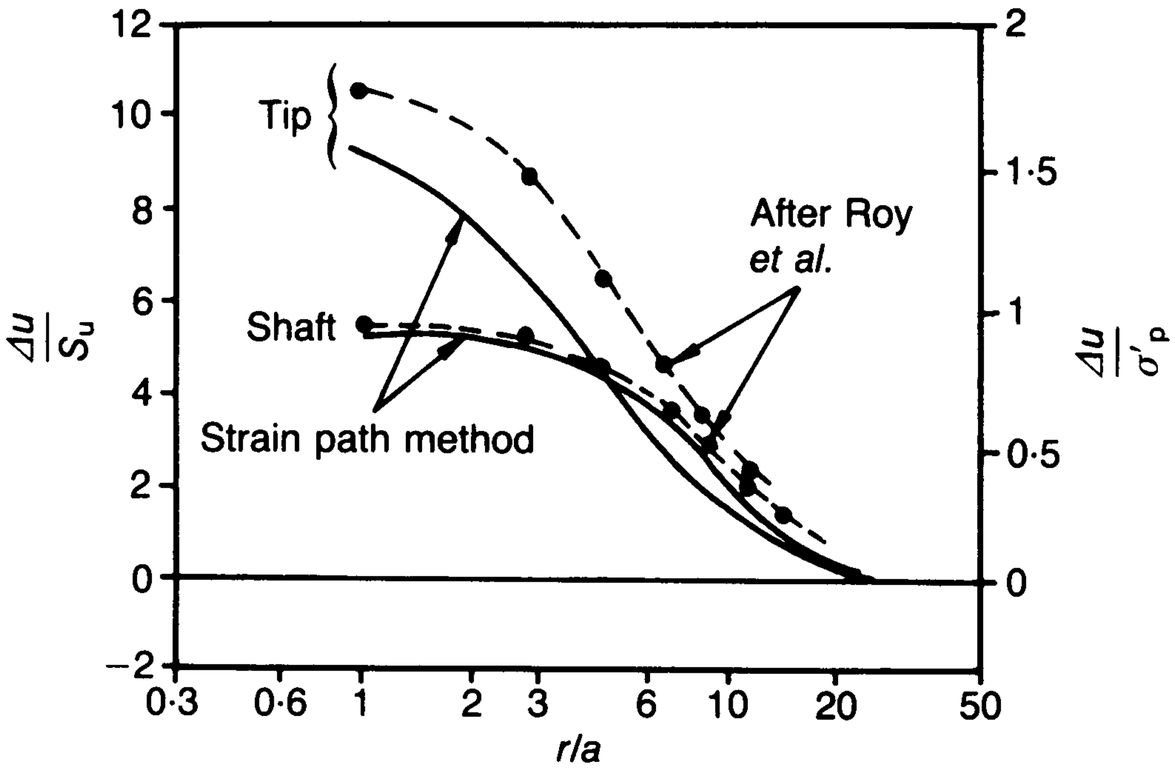

Fig. 16. Excess pore water pressure due to deep penetration

The excess pore pressure developed during the installation of the piezometer was allowed to dissipate before the test began. The reader is referred to the original publication for further details.

The variation of $\Delta u/\sigma_p'$, where σ_p' is the effective preconsolidation pressure, from one of the tests is shown in Fig. 16. The normalized excess pore pressure derived from the strain path method is plotted in the same figure as $\Delta u/s_u$. The computation was based on an I_r value of 300, which is estimated from the data presented by Roy *et al.* If it is accepted that s_u can be correlated to σ_p' via a simple linear relationship, then Fig. 16 indicates that there is good qualitative agreement between the computed and experimental results regarding the variation of excess pore pressure with radial distance. This is significant as the rate of excess pore pressure dissipation is dependent on the gradient of Δu, rather than the absolute values, in a linear consolidation analysis.

The computed Δu is used as the initial condition in a dissipation analysis based on the Terzaghi–Rendulic uncoupled consolidation theory. It is recognized that this theory involves the important approximation of no change of total stress during consolidation. This is known not to be true, nevertheless the uncoupled theory can provide some insight into the consolidation process. A fully coupled analysis would be very considerably more complex. The governing equations of the uncoupled consolidation theory are discretized and solved using an alternating direction implicit finite difference scheme. The pore pressure at different stages of dissipation is shown in Fig. 17. The initial pore pressure distribution is based on an I_r value of 100. The time factor T is defined as

$$T = \frac{c_h t}{a^2} \tag{32}$$

where c_h is the coefficient of consolidation in the horizontal direction and t is the time. It was observed that the high pore pressure around the cone tip dissipates rapidly. Further up the cone shaft the pore pressure only begins to decrease after a small lapse of time. In fact at some locations above the cone shoulder Δu was found to increase slightly initially due to the pore pressure redistribution from the high pressure region around the tip. In regions where the excess pore pressure increases (and since total stress is assumed constant mean effective stress therefore reduces) the coefficient of swelling is taken as being the same as the coefficient of consolidation. This initial redistribution process is followed by a gradual dissipation of Δu at all locations. Note that the steep gradient of Δu at $T = 0$ near the shoulder may indicate a disadvantage in placing the piezometer at this location, in that the interpretation of the data may not be straightforward.

The dissipation calculation has been repeated using different ratios of the horizontal and vertical consolidation coefficients. The profile of the resulting dissipation curves are generally similar

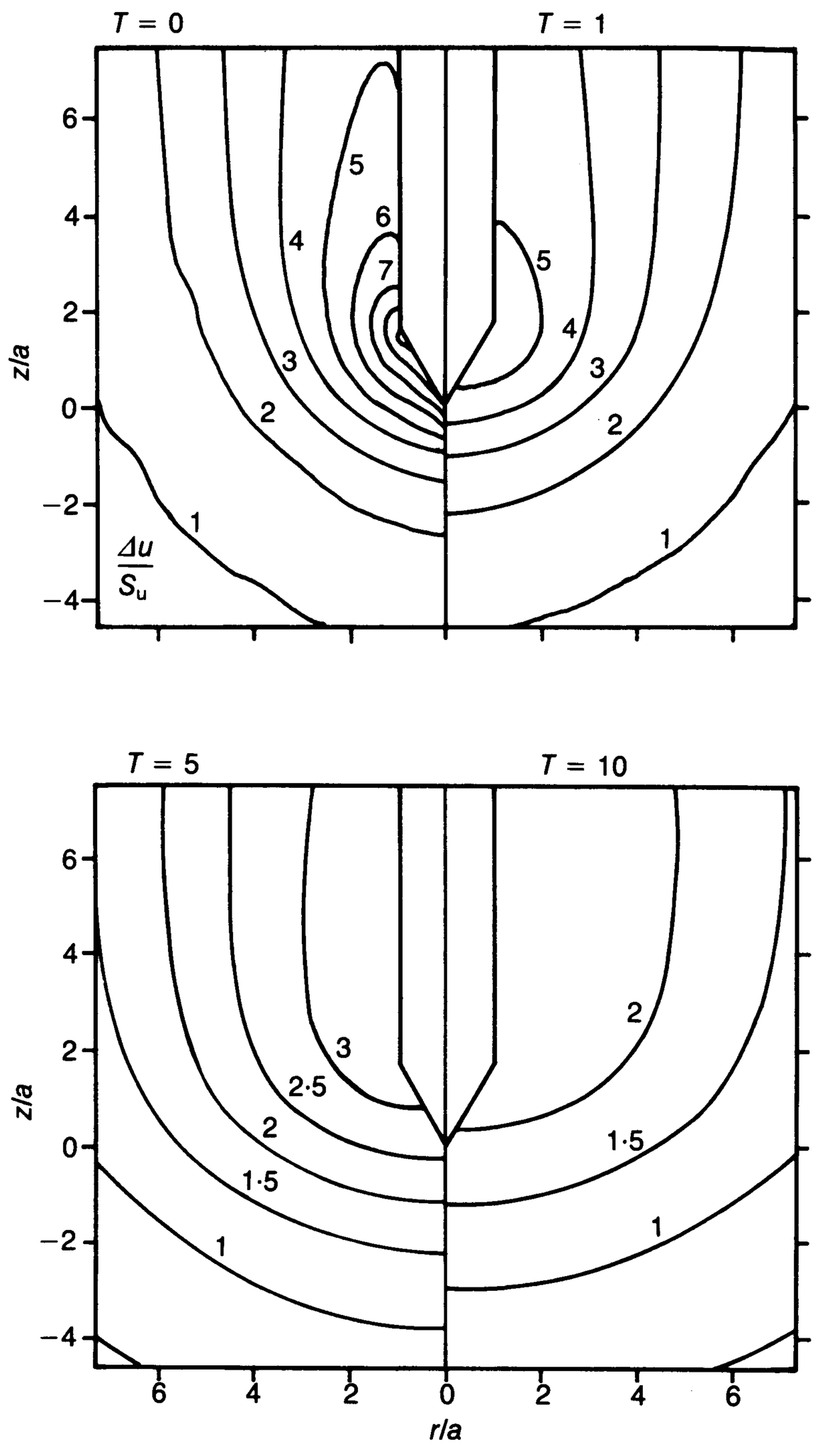

Fig. 17. Distribution of pore water pressure at various stages of dissipation

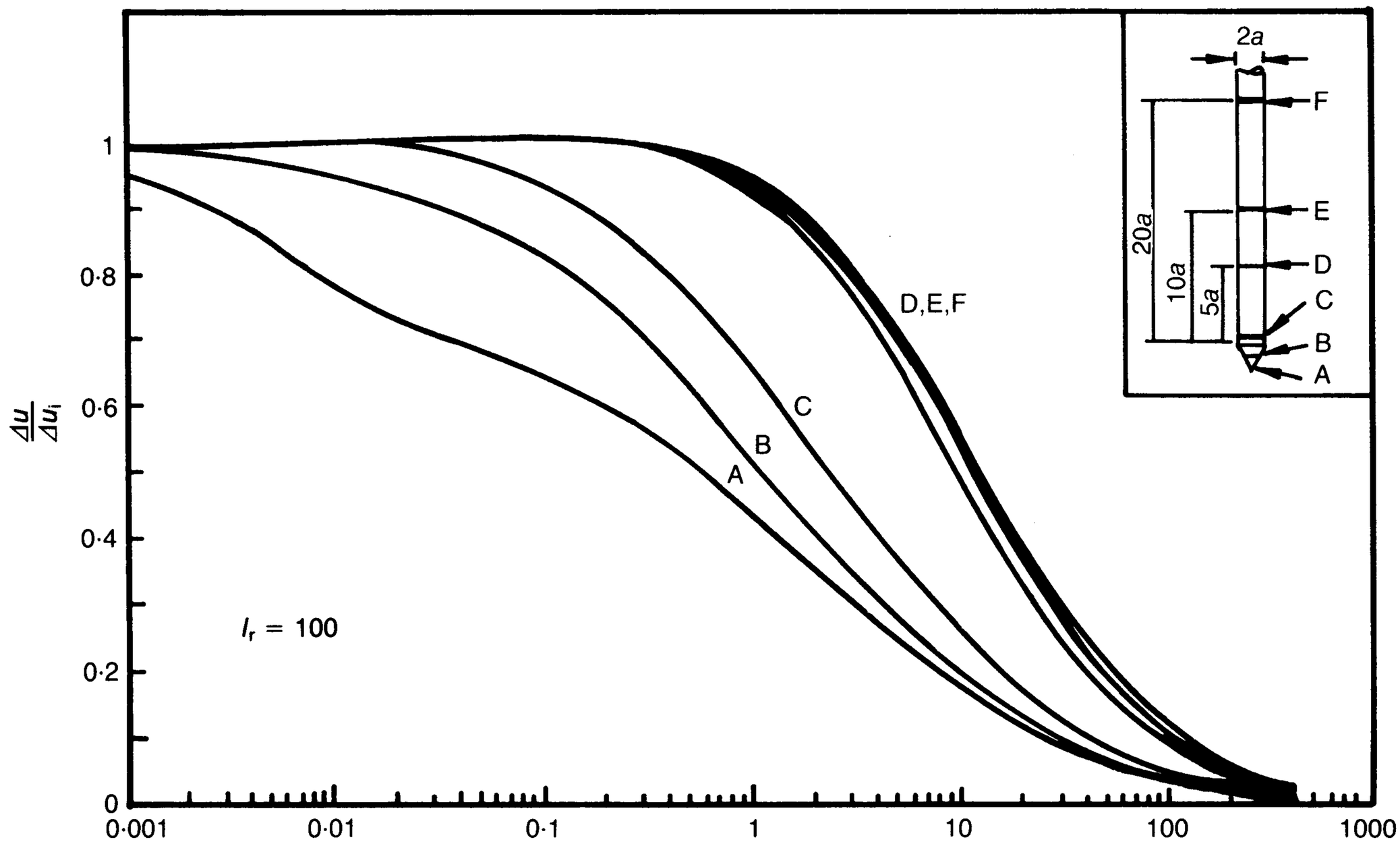

Fig. 18. Dissipation curves at different locations of a 60° cone penetrometer

to those for the isotropic case. For $c_h > c_v$, the consolidation behaviour is dominated by c_h, with c_v having negligible effect.

Figure 18 shows the non-dimensional dissipation curves of excess pore pressure against T on a logarithmic scale at six different locations along the penetrometer. The locations labelled A to F correspond to the cone tip, mid-way between tip and shoulder, cone shoulder, and locations at 5, 10 and 20 cone radii above the shoulder respectively. The results are comparable to dissipation curves from previous studies (e.g. Torstensson 1977, Randolph & Wroth, 1979) except for the dissipation at location A, which shows an unusual response due to the special conditions prevailing at the cone tip.

Unfortunately, these dissipation curves are not unique, since the initial pore pressure distribution is dependent on the value of I_r. In particular, the size of the zone of soil surrounding the penetrometer in which excess pore pressures develop varies with I_r. For the constitutive model assumed this zone corresponds approximately to the plastically deforming region which can be characterized by r_p and z_p. From a theoretical point of view it would be more rational (though less convenient) to choose a dimension related to the zone subjected to excess pore pressure (for example $a\sqrt{I_r}$) rather than the cone radius a in the definition of T. If this is adopted it would result in a new time factor T'

$$T' = \frac{c_h t}{a^2 I_r} \tag{33}$$

However, this definition of T does not adequately account for the many other factors which govern the dissipation process. These factors include the differences in pore pressure gradients due to different I_r values and the fact that the location of the zero pore pressure line changes as the dissipation proceeds. In fact it has been determined empirically that the most satisfactory way of unifying the results at different I_r values is obtained if the time factor is defined as

$$T^* = \frac{c_h t}{a^2 \sqrt{I_r}} \tag{34}$$

When the dissipation results are plotted using this time factor, the dissipation curves for all values of I_r from 25 to 500 are very satisfactorily unified. Fig. 19 shows the dissipation curves at the cone face and the cone shoulder. The small difference between the dissipation curves for different I_r values clearly demonstrates the advantages of using T^* instead of T. Previous analyses of this problem (e.g. Baligh & Levadoux, 1985) have taken no account of the important influence of soil shear stiffness on the consolidation process.

Based on these results, the modified time factors at various stages of dissipation as shown in Table 2 are obtained. The time factors in Table 2 have been compared with previous analytical studies of consolidation which were based on cylindrical cavity expansion theory (uncoupled analysis by Torstensson, 1977, and coupled analysis by Randolph & Wroth, 1979). Taking

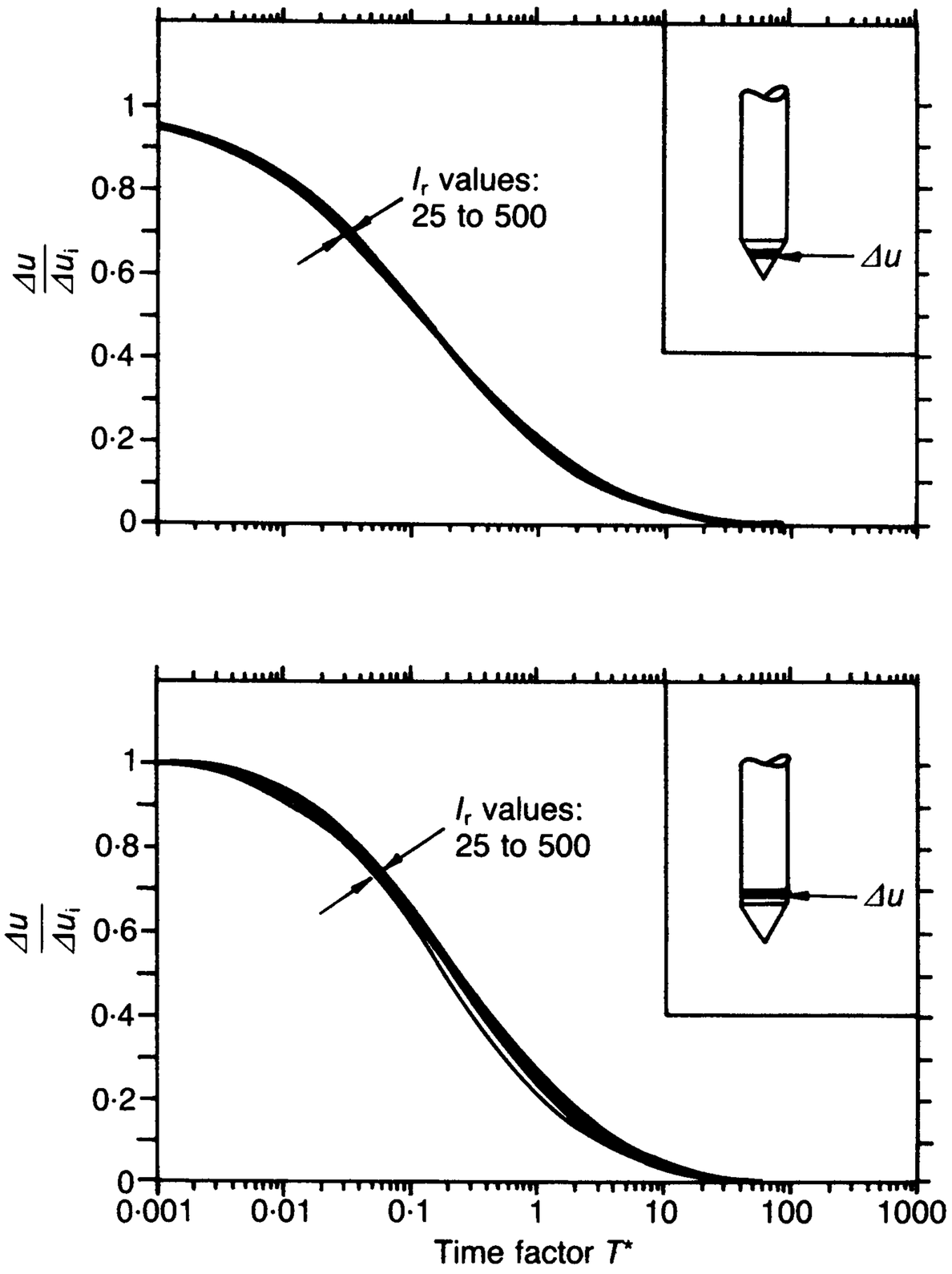

Fig. 19. Normalized dissipation curves plotted against T^*

account of the different I_r values used in these analyses, it is found that the consolidation rate at the shoulder is very similar to the solutions based on cylindrical cavity expansion. At the tip the new analysis predicts faster dissipation and on the shaft (5 to 10 radii above cone shoulder) the dissipation is predicted to be considerably slower than that given by cavity expansion theory. The explanation of these differences lies in the fact that the gradient of mean stress with radius near the cone shoulder compared closely with cylindrical cavity expansion theory (Teh, 1987). On the shaft the initial pore pressures are lower and gradient with pore pressure much flatter, leading to a slower rate of dissipation. This is related to a slight unloading of the soil which occurs behind the cone shoulder. In addition the consolidation process is further delayed by redistribution of high pore pressures from the tip region.

An alternative way of presenting the dissipation data is the root time plot, where the initial section of the dissipation curve usually approximates closely to a straight line. It is useful to present dissipation data in this manner when only a short dissipation record is available. When plotted against $\sqrt{T^*}$ the initial portion of the computed dissipation curves has indeed been found to be linear. The gradients of these linear sections of the dissipation curves for three locations along the penetrometer are given in Table 3. These results are applicable for I_r in the range 50 to 500.

CONCLUSIONS

In this Paper, the analysis of the cone penetrometer using the strain path method has been presented. Due to the approximate strain field assumed, the derived stresses imply a small error in equilibrium. Several methods have been attempted in order to correct this error iteratively but none of these have been completely successful. An alternative approach which incorporates the merits of the strain path method and the finite element method has been presented.

Table 2. Time factor at different stages of dissipation

	Modified time factors T^*				
Degree of consolidation	Cone tip	Cone face	Cone shoulder	5 radii above cone shoulder	10 radii above cone shoulder
20%	0·001	0·014	0·038	0·294	0·378
30%	0·006	0·032	0·078	0·503	0·662
40%	0·027	0·063	0·142	0·756	0·995
50%	0·069	0·118	0·245	1·11	1·46
60%	0·154	0·226	0·439	1·65	2·14
70%	0·345	0·463	0·804	2·43	3·24
80%	0·829	1·04	1·60	4·10	5·24

Table 3. Initial slopes for dimensionless root time plots

Location	Cone tip	Cone face	Cone shoulder	5 radii behind cone shoulder
Gradient	1·30	1·63	1·15	0·62

The theoretical values of cone factor N_{kt} have been derived. The cone factor was found to be influenced significantly by the rigidity index of the soil and the in-situ stress conditions. In addition, it is evident from the analysis that the in-situ horizontal stresses have a greater influence on the cone factor than the vertical stress. To a lesser extent the roughness of the cone and shaft also affect the tip resistance. Based on the results of the analyses an approximate expression for the cone factor in terms of these parameters has been proposed.

Dissipation of pore pressure around the cone is primarily governed by the horizontal permeability. The dissipation curves vary depending on the location of the piezometric element. The excess pore pressure generated is found to be dependent on I_r. In order to provide a consistent interpretation method it is necessary to redefine the time factor to account for the effect of rigidity index. Such a time factor has been proposed and dissipation curves which are almost unique have been obtained for various locations along the penetrometer. Based on these computed dissipation results time factors at different degrees of consolidation have been suggested. An alternative interpretation method based on the gradient of the dissipation curve plotted as normalized excess pore pressure against $\sqrt{T^*}$ has also been proposed. The latter technique is useful when only a short dissipation record is available.

The results of both the penetration analysis and the consolidation analysis demonstrate the important influence of the rigidity index I_r on the interpretation of the penetration data. If the cone penetration test is to be interpreted rationally, then information about soil stiffness is necessary. While this may be inconvenient, it cannot be ignored.

ACKNOWLEDGEMENT

This work was carried out while the first author was a research student at Oxford University supported by the Kuok Foundation, Malaysia. Additional resources were provided by the Science and Engineering Research Council. The authors are grateful to many of their colleagues for valuable discussions and particularly to Professor C. Sagaseta of the University of Cantabria, Santander, Spain.

APPENDIX I

The stresses derived using the strain path method do not fully satisfy the equilibrium condition because of the error in the assumed initial displacement field. In principle, if one equilibrium equation has been used to compute the mean pressure then the other may be used to obtain an adjustment to the displacement field so that an improved estimate is obtained. This process can then be repeated iteratively to arrive at a converged solution which satisfies the equilibrium condition. In the course of this research the following schemes have been adopted to attempt this correction.

Newton–Raphson correction

By cross differentiating the equilibrium equations they may be combined to eliminate the mean stress

$$\frac{\partial}{\partial z}\left[\frac{\partial \sigma_{rr}'}{\partial r}+\frac{\partial \tau_{rz}}{\partial z}+\frac{\sigma_{rr}'-\sigma_{\theta\theta}'}{r}\right]$$

$$-\frac{\partial}{\partial r}\left[\frac{\partial \tau_{rz}}{\partial r}+\frac{\partial \sigma_{zz}'}{\partial z}+\frac{\tau_{rz}}{r}\right]=H \quad (35)$$

where H is identically zero for a set of stresses in equilibrium and is taken as a measure of the error for a set of stresses which are not in equilibrium.

An initial set of the stream function value Ψ_0 is estimated and the corresponding values of H_0 determined. At each finite difference grid point Ψ is then perturbed by a small amount, and the resulting effect on H evaluated at every other grid point. The changes in H are confined to a region 'downstream' and extending a small distance to either side of the perturbed point. By repeating this process at every grid point an $N \times N$ matrix (where N is the number of grid points in the finite difference mesh) of 'partial derivatives' of H with respect to Ψ can be calculated. By multiplying the vector $-H_0$ by the inverse of this matrix the correction to Ψ which is needed to eliminate the error approximately (or exactly in the case of a linear problem) may be determined.

The calculation is then repeated with the new set of Ψ values until the error is reduced to a satisfactory level. Testing of this approach with some simple problems showed that as long as the perturbed flow does not include any regions in which plastic deformation occurs then the method converges very rapidly on the correct solution. This is because the equations are purely linear in these cases. If, however, there is any plastic deformation, as is the case for all realistic cone penetration problems, then the method does not converge (even when acceleration or deceleration techniques are also adopted).

Pseudo-dynamic correction

The second correction method is based on an unsteady flow approach. In this case the equilibrium equations are considered for a material with density ρ

$$\frac{\partial \sigma_{rr}}{\partial r}+\frac{\partial \tau_{rz}}{\partial z}+\frac{\sigma_{rr}-\sigma_{\theta\theta}}{r}=\rho\left[\frac{\partial u}{\partial t}+u\frac{\partial u}{\partial r}+v\frac{\partial u}{\partial z}\right] \quad (36)$$

and a similar equation in the vertical direction. Introducing the vorticity $\xi=(\partial u/\partial z)-(\partial v/\partial r)$ and again cross differentiating the modified equilibrium equations to eliminate the mean stress leads, after some manipulation, to the equation

$$\frac{\partial \xi}{\partial t}=\frac{H}{\rho}-\left[u\frac{\partial \xi}{\partial r}+v\frac{\partial \xi}{\partial z}-\frac{u\xi}{r}\right] \quad (37)$$

which is a form of the vorticity transport equation.

A choice of a sufficiently small value of ρ can always be made so that the bracketed term in equation (37) is small relative to H/ρ. By adopting a small time step the value of H may be used to calculate an increment of ξ, which in turn serves as a source term in the equation

$$\xi = -\frac{1}{r}\frac{\partial^2\psi}{\partial r^2} - \frac{1}{r}\frac{\partial^2\psi}{\partial z^2} - \frac{1}{r^2}\frac{\partial\psi}{\partial r} \tag{38}$$

to determine a new field of Ψ values. Equation (38) arises from the definition of ξ and equation (10). Equation (38) is solved using the successive over-relaxation technique.

While this method might be expected to be robust it has been found so far that, in spite of the choice of a wide variety of densities and time steps, the method reduces major errors but does not eliminate the inequilibrium completely.

Finite element correction

The third scheme considered involved the use of finite element analysis. The stresses from the strain path method were passed to a finite element program and the equivalent out-of-balance forces calculated. These forces were then negated in a conventional incremental analysis. The corresponding displacements were considered as indicating the shift in the streamline pattern and the updated streamlines were then used to compute a new strain path solution. While not based on any rigorous interpretation it was considered that this approach, which involves arriving at an equilibrium solution albeit by an 'incorrect' stress path, could lead to a workable correction scheme. The scheme did not in fact work but this is thought to be due, at least in part, to difficulties in the interpolation of stresses between the rectangular mesh used for the strain path method and the Gauss points in the triangular mesh used in the finite element analysis (this choice was made for reasons beyond the scope of this Paper). Even when no correction was carried out the two stages of interpolation result in small stress changes. It remains to be seen whether the method might be successful with more closely matched grids for the two numerical schemes. In addition the problem of interpolation might be overcome if a single numerical scheme is adopted for the strain path calculation and the subsequent correction procedure. This will be the goal of future research effort.

NOTATION

a	cone radius
c_h	horizontal coefficient of consolidation
c_v	vertical coefficient of consolidation
E_1, E_2, E_3	strain invariants
G	shear modulus of soil
H	error of inequilibrium
I_r	rigidity index
N_h	cone factor defined in terms of σ_{ho}
N_{kt}	cone factor
N_s	spherical cavity expansion factor
p	mean normal stress
p_r	mean normal stress evaluated using radial equilibrium equation
p_p	mean normal stress evaluated from Poisson's equation
q_t	cone resistance
r, z, θ	components of a cylindrical co-ordinate system
r_p, z_p	location of elastic–plastic radius
s_u	undrained shear strength in triaxial compression
t	time
T	dimensionless time factor
T', T^*	modified time factor
u, v	velocity components in the r and z directions
α	pore water pressure parameter
α_f	roughness factor on the cone face
α_s	roughness factor on the cone shaft
β	cone tip angle
γ_{oct}	octahedral shear strain
Δ	in-situ stress factor
Δu	excess pore water pressure
Δu_o	initial excess pore water pressure
δ_{ij}	Kronecker delta
$\varepsilon_{rr}, \varepsilon_{\theta\theta}, \varepsilon_{zz}, \gamma_{rz}$	strain components
$\dot{\varepsilon}_{rr}, \dot{\varepsilon}_{\theta\theta}, \dot{\varepsilon}_{zz}, \dot{\gamma}_{rz}$	strain rate components
λ	plastic multiplier
ξ	vorticity
ρ	density
σ_{ho}, σ_{vo}	in-situ horizontal and vertical stress
σ_p'	effective preconsolidation pressure
σ_{oct}	octahedral normal stress
σ_{ro}	in-situ radial stress in cavity expansions
$\sigma_{rr}, \sigma_{zz}, \sigma_{\theta\theta}, \tau_{rz}$	components of stress
$\dot{\sigma}_{\theta\theta}, \dot{\tau}_{rz}$	components of stress rate
$\sigma_{rr}', \sigma_{zz}', \sigma_{\theta\theta}', \tau_{rz}'$	deviatoric stress components
τ_{oct}	octahedral shear stress
Ψ	stream function
Ψ_c	limit pressure in cylindrical cavity expansion
Ψ_s	limit pressure in spherical cavity expansion

REFERENCES

Baligh, M. M. (1985). Strain path method. *J. Geotech. Engng Div., Am. Soc. Civ. Engrs* **111,** No. 9, 1109–1135.

Baligh, M. M. (1986). Undrained deep penetration, I: shear stresses. *Géotechnique* **36,** No. 4, 471–485.

Baligh, M. M. & Levadoux, J. N. (1985). Consolidation after undrained piezocone penetration II: interpretation. *J. Geotech. Engng* **112,** No. 7, 727–745.

Cox, A. D., Eason, G. & Hopkins, H. G. (1961). Axially symmetric plastic deformation in soils. *Trans. Royal Soc. London*, Ser. A. **254,** 1–45.

De Borst, R. & Vermeer, P. A. (1984). Possibilities and limitations of finite element for limit analysis. *Géotechnique* **34,** No. 2, 199–210.

Henkel, D. J. (1959). The relationship between the strength, pore water pressure and volume change characteristics of saturated clays. *Géotechnique* **9,** No. 3, 199–235.

Houlsby, G. T. & Wroth, C. P. (1982). Determination of undrained strength by cone penetration tests. *Proc.*

2nd European Symp. on Penetration Testing, Amsterdam, **2**, 585–590.

Houlsby, G. T. & Wroth, C. P. (1983). Calculation of stresses on shallow penetrometers and footings. *Proc. IUTAM/IUGG Symp. on Seabed Mechanics*, Newcastle, 107–112

Houlsby, G. T., Wheeler, A. A. & Norbury, J. (1985). Analysis of undrained cone penetration as a steady flow problem. *Proc. 5th Int. Conf. Num. Meth. in Geomech.*, Nagoya, Japan, **4**, 1767–1773.

Kiousis, P. D., Voyiadjis, G. Z. & Tumay, M. T. (1988). A large strain theory and its application in the analysis of the cone penetration mechanism. *Int. J. Num. Anal. Meth. in Geomech.*, **12**, No. 1, 45–60.

Koumoto, T. & Kaku, K. (1982). Three-dimensional analysis of static cone penetration into clay. *Proc. 2nd European Symp. on Penetration Testing*, Amsterdam, **2**, 635–640

Norbury, J. & Wheeler, A. A. (1987). On the penetration of an elastic–plastic material by a slender body. *Q. J. Mech. Appl. Math.* **40**, No. 4, 477–491.

Randolph, M. F. & Wroth, C. P. (1979). An analytical solution for the consolidation around a driven pile. *Int. J. Num. Anal. Meth. in Geomech.* **3**, No. 3, 217–229.

Roy, M., Blanchet, R., Tavenas, F. & La Rochelle, P. (1981). Behaviour of a sensitive clay during pile driving. *Can. Geotech. J.* **18**, 67–86.

Sagaseta, C. (1985). Private communication.

Sagaseta, C. & Houlsby, G. T. (1988). Elastic incompressible flow around an infinite cone. *Proc. 1st Int. Symp. on Penetration Testing*. Orlando, **2**, 933–938.

Sloan, S. W. & Randolph, M. F. (1982). Numerical prediction of collapse loads using finite element methods. *Int. J. Num. Anal. Meth. Geomech.* **6**, 47–76.

Teh, C. I. (1987). *An analytical study of the cone penetration test*. DPhil thesis, Oxford University.

Torstensson, B.-A. (1977). The pore pressure probe. *Nordiske Geoteknisk Mote*, Oslo, Paper No. 34.

Vesic, A. S. (1972). Expansion of cavities in infinite soil mass. *J. Soil Mech. Fndn. Engng Div., Am. Soc. Civ. Engrs* **98**, 265–290.

Teh, C. I. & Houlsby, G. T. (1992). *Géotechnique* **42,** No. 3, 529–532

DISCUSSION

An analytical study of the cone penetration test in clay

C. I. TEH and G. T. HOULSBY (1991). *Géotechnique* **41,** No. 1, 17–34

M. Fahey, *University of Western Australia,* **and A. Lee Goh,** *Main Roads Department of Western Australia*

The Authors have presented very interesting and useful analyses of the cone penetration test in clay and of the generation and dissipation of pore pressure around the cone when penetration is halted. These analyses appear to constitute a significant advance in the interpretation of the cone test.

Over the past few years, we have been studying the dissipation phase of the cone test with a view to using the test to determine the coefficient of consolidation for soft clay. Some aspects of the Authors' analysis are now examined in the light of data from this study.

The study concentrated on a soft alluvial clay deposit of recent origin located on Burswood Peninsula, formed in a meander of the Swan River in Perth, Western Australia. The clay has a liquid limit ranging from 105 to 125 and a plasticity index ranging from 70 to 95, and is normally consolidated or very lightly overconsolidated. Vane, cone penetration and self-boring pressuremeter tests have also been conducted at the site. The pressuremeter tests consisted of normal expansion tests and also strain-holding and pressure-holding tests to examine the pore pressure dissipation. Triaxial and oedometer test data are also available.

The cone penetrometer used in the study was designed specifically to examine the dissipation process. The present cone is the third in a series, the first two having been described by Fahey & Foley (1987), and the third by Lee Goh & Fahey (1991). In all three versions, the cone diameter is 40 mm, and the cone angle can be varied (although in fact only angles of 12° and 60° were used). The pore pressure measurement was usually at a point 4 diameters behind the cone shoulder, although by inserting or removing spacers, this point could be made as close as 1·5 diameters behind the cone shoulder. None of the cones incorporated the standard cone features of measurement of q_c or f_s. The other main features of the cones were as follows.

(*a*) *Cone 1.* Pore pressure measurement was via a pressure transducer located in the centre of the body. Pore pressure in the soil was transmitted through a thin annular sintered stainless steel filter to a thin annular space behind the filter, and thence via two small diameter holes to a small chamber in front of the sensing face of the transducer.

(*b*) *Cone 2.* Two miniature Druck pore pressure transducers with sintered stainless steel filters were used in the second cone. These were located at 180° separation on the body. The main design criterion was to make the water volume between the filter and the transducer as small as possible.

(*c*) *Cone 3.* The additional feature of this cone is that each of the two Druck pore pressure transducers is located in the centre of the sensing element of a total radial stress transducer, thereby allowing both pore pressure and total stress (and hence effective stress) to be measured simultaneously at two diametrically opposite points at all stages of cone penetration and pore pressure dissipation.

From an experimental point of view, one of the findings from the study is that it is extremely difficult to obtain sufficiently fast response from pore pressure transducers to obtain an accurate picture of what happens during cone penetration in clay, and immediately after halting penetration. As the design of the cones improved (from cone 1 to cone 3), and as experience in methods of de-airing improved, the transducer response also improved. The de-airing technique consisted of placing an air-tight sleeve around the cone, and cycling the water pressure in the sleeve between ± 100 kPa. A cased borehole was augured to the water table, and this hole was filled with water. The sleeve was removed from the cone only after the cone had been immersed in the water of the borehole. When cone penetration was halted, the time taken for the pore pressure readings to reach a peak was taken as a measure of the response. In other words, the lag in response was taken to be due more to a deficiency with the measuring